Feeder Link Precoding for Future Broadcasting Services: Architecture and Performance

Feeder Link Precoding for Future Broadcasting Services: Architecture and Performance

Alessandro Guidotti, *Member, IEEE,* Claudio Sacchi, *Senior Member, IEEE,*
and Alessandro Vanelli-Coralli, *Senior Member, IEEE*

***Abstract*—5G systems are becoming a reality and the evolution towards Beyond 5G (B5G) and 6G systems is already being defined, also to cope with the ever increasing capacity demanded by on-ground users. This will pose challenging requirements on the feeder link of future satellite systems, which risks to become a bottleneck for the overall system performance. In this paper, we propose a novel architecture of linear precoding for the feeder link of a broadcast satellite system operating with full frequency reuse to significantly enhance the achievable capacity. The architecture has been simulated and tested in a challenging multi-frequency scenario, where Ku, Ka, Q/V, and W band have been considered for transmission. The numerical performance analysis and the open issues related to the practical realisation of the proposed architecture are also thoroughly discussed.**

***Index Terms*—Architecture, Communication system performance, Atmospheric propagation, MIMO systems, Broadcasting**

I. Introduction

NEtwork analyses foresee that by 2023 there will be 5.3 billions Internet users and almost 30 billions devices, [1]. Among these, video devices are expected to have a multiplier effect on the traffic demand. For instance, an Internet-enabled TV set will generate as much traffic as that of an entire household today; taking into account that $\approx$ 900 millions TV sets with 4K capabilities are expected by 2023 and that Ultra High Definition (UHD) Virtual Reality (VR) is likely to become one of the most requested services, it is clear that the current feeder link resources and structure cannot satisfy the requested aggregate traffic anymore, thus risking to become the system bottleneck.

In terms of satellite broadcasting systems, legacy networks rely on a star topology with point-to-multipoint links, in which, [2], [3]: i) a transmitting hub station, equipped with a rather large antenna, is the central transmitting node and it offers Direct To Home (DTH) services through a single feeder link; and ii) the User Terminals (UTs) are typically receive-only stations, with a limited antenna size so as to limit their cost, served through a large single wide-area user beam providing regional coverage (*e.g.*, Europe). The network hub is located either at the broadcaster's facilities, and thus it is operated by the broadcaster itself, or in some other location, at which it is often managed by the satellite network operator. The potential exploitation of EHF bands in such traditional broadcast networks was preliminarily discussed in [4], where it was correctly pointed out by the authors that: i) on the feeder link, EHF bands might be used, as long as proper site diversity is achieved by means of multiple GWs in order to contrast the large propagation impairments; and ii) on the user link, atmospheric phenomena would be too disruptive due to the lack of transmit diversity techniques, thus leading to the possible need for a backup user beam connection at lower frequencies. In this context, it is worth highlighting that the use of a single wide beam on the user link might not be sufficient for future broadcasting services, due both to the large bandwidth requirements to provide Ultra-High Definition TV (UHDTV) or 8K UHDTV services to the general public and to the increasing need for on-demand dedicated content, to be provided by means of unicast or multicast connections to the users' set-top boxes. In the framework of multi-beam coverage on the user link, the deployment of multiple GWs is beneficial not only to implement site diversity, but also to actually manage the multi-beam user coverage, with each GW managing the traffic of a different subset of beams.

Based on the above observations and on the successful deployment of High Throughput Satellite (HTS) systems, further evolving into Very HTS (VHTS), more advanced architectures and transmission techniques can be envisaged so as to fully benefit from the potential of the EHF bandwidth. In this paper, we focus on broadcasting services provided through a HTS/VHTS Geostationary Earth Orbit (GEO) satellite with multi-beam coverage on both the feeder and user links. Aiming at the full exploitation of the large feeder bandwidth in EHF, and in order to cope with the larger capacity requirements that future broadcasting services will pose on the system, full frequency reuse is implemented on the feeder link. Notably, due to the antenna radiation pattern sidelobes, proper interference management techniques are required in order to cope with adjacent beam interference. These can be implemented at the receiver side (the satellite, in our scenario), as Multi-User Detection (MUD) [5], or at the transmitter (the GWs), as precoding. We focus on the implementation of precoding techniques at the GWs, so as to avoid any increase in the payload complexity, which would also lead to an increased cost in terms of manufacturing and launch into orbit. Since the GWs are geographically separated so as to guarantee site diversity,

A. Guidotti is with the Department of Electrical, Electronic, and Information Engineering, University of Bologna, 40136 Bologna, Italy, and with the Consorzio Nazionale Inter-Universitario per le Telecomunicazioni, Research Unit at the University of Bologna, 43124 Parma, Italy (e-mail: a.guidotti@unibo.it).

C. Sacchi is with the Department of Information Engineering and Computer Science, University of Trento, 38133 Trento, Italy, and also with the Consorzio Nazionale Inter-Universitario per le Telecomunicazioni, Research Unit at the University of Trento, 43124 Parma, Italy (e-mail: claudio.sacchi@unitn.it)

A. Vanelli-Coralli is with the Department of Electrical, Electronic, and Information Engineering, University of Bologna, 40136 Bologna, Italy (e-mail: alessandro.vanelli@unibo.it).

Manuscript received xxxx; revised August xxxx.

they can be considered as distributed antennas that implement the precoding weights computed by a central network entity. In this context, we thoroughly define the system architecture in terms of the ground segment and required functional and signalling information to actually implement precoding with distributed GW antennas and then extensively discuss on the advantages and disadvantages that such approach can bring into the considered system in terms of average spectral efficiency and overall system capacity.

A. Literature review

The State-of-the-Art (SoA) framework of the present paper is comprehensive of three main topics: future HTS systems, precoding techniques applied to multi-beam satellites, and multicast precoding techniques.

The recent literature dealing with HTSs is rich of contributions targeted at increasing the system capacity in the presence of atmospheric impairments and other link non-idealities. In the paper from Roumeliotis *et.al.*, [6], a dynamic capacity allocation scheme based on matching theory is proposed, which provides a low complexity optimum allocation based on capacity loss metric of paired user beams and gateways. A work related to [6] is [7], where a theoretically optimum capacity allocation scheme based on Monge arrays is discussed targeted at optimising system capacity losses and rate matching performance metrics. Another very recent work, [8], investigates the impact of distortions involved by on-board transponder filters and high-power amplifiers on the HTS performance. A method based on digital pre-distortion is proposed in [8] in order to counteract these typologies of distortions and improve the overall link performance. The integration of HTS with 5G systems is considered in [9]; in this paper, the HTS is regarded as a master node capable of providing efficient and transparent backhaul to the disperse broadband network segments typical of 5G.

As far as the exploitation of EHF bands is concerned, some contributions presented in the literature address the assessment of broadband transmission solutions in terms of link performance and achievable raw capacity, [10], [11]. Other studies are focused on the design of waveforms capable at providing resilience against the typical impairments of the EHF Radio-Frequency (RF) environment, [12]–[14], where the performance is usually limited by non-linear distortions and phase noise. In [15], the authors focus on the application of Adaptive Coding and Modulation (ACM) for EHF satellite communications, by optimising the DVB-S2 thresholds and including rain fading and the non-linearities of the on-board amplifiers. The authors of [16] discuss on the exploitation of the EHF large bandwidths for HDTV broadcasting services, again following the DVB-S2 specifications and also including phase noise. In [4], the authors report a detailed survey of the opportunities and challenges of EHF transmissions for broadcasting services, also providing a detailed theoretical evaluation of the achievable capacity compared to Ku/Ka bands. In addition to the above manuscripts, the literature on EHF also presents many pioneering feasibility studies, as those in [17] and [18], reporting the DAVID and WAVE experiments, respectively. In [19], [20], the authors report some of the results achieved by more recent EHF experiments, like, *e.g.*, the ALPHASAT measurement campaign in Q/V-band. Following such a trend, in [21], the authors address the exploitation of Q/V bands with gateway diversity on the feeder link, showing the significant gains that can be obtained with proper ground segment configurations and switching schemes.

With respect to precoding-based Satellite Communication systems (SatCom), the literature is quite extensive thanks to the last years of research exploiting the successful implementation in terrestrial systems, [22], but mainly addressing its implementation on the user forward link. Initial implementations of precoding to satellite systems were based on the extension of Multi-User Multiple Input Multiple Output (MU-MIMO) approaches, which already showed good performance in terrestrial communications, moving to Zero-Forcing (ZF) and Minimum Mean Square Error (MMSE) algorithms, [23]; the throughput gains on both the Forward Link (FL) and the Return Link (RL) of the considered multi-beam satellite system can be as large as 80%. A valuable survey on MIMO techniques implemented over satellite channels is provided in [24], where the authors discuss both fixed and mobile satellite systems and identify the major impairments related to the channel, paving the way for future research activities. The main technical challenges when moving precoding to a SatCom context are discussed in [25], in particular the impact of partial Channel State Information (CSI) at the transmitter side; in this work, the authors propose a novel precoding scheme to increase the system sum-rate and availability. The implementation of precoding to systems based on the DVB-S2X standard was also discussed in the context of several European Space Agency (ESA) R&D activities in [26]; more specifically, practical challenges arising when implementing precoding in HTS systems were discussed, as framing issues, non-ideal (*i.e.*, outdated) phase estimates, imperfect channel estimation, and multiple gateways. Still related to practical impairments for precoding in DVB-S2X, extensive analyses have been provided in [27]; in addition, in [28]- [29], a thorough review of precoding techniques for multi-beam systems is provided. In addition, optimisations for the precoding design with linear and non-linear power constraints are proposed. In [30], the non-linear Tomlinson-Harashima precoding (THP) is proposed, which is based on modulo operations over the symbols constellation by taking into account the beam gain as well. The performance of linear beamforming in terms of the fulfilment of specific traffic demands is discussed in [31], where the authors proposed to include generic linear constraints in the transmit covariance matrix, obtaining gains with respect to traditional frequency reuse approaches as large as 170%. In [32], the authors discuss on-board precoding solutions for multiple gateway systems, proposing solutions to mitigate inter-beam and inter-FL interference. In [33], the authors consider a Licensed Shared Access (LSA) system in which both satellite and terrestrial wireless service providers share a given frequency band and focus on the precoding scheme restricting the received power of the satellite UTs to be under a certain threshold. The authors of [34] optimise the precoded system at the receiver side in terms of Signal-to-

Noise Ratio (SNR), whilst guaranteeing the system fairness and allowing a control over the power transmitted by each antenna, in particular reducing the power peaks. In [35], the focus is on precoding applied to a hot-spot cell configuration encompassing a random user distribution in the service area. In [36], the authors introduce the concept of beam-free systems and investigate the advantages obtained when the scheduling algorithm is able to freely group users independently of their beam location. The authors of [37] focus on the performance of precoded multi-beam systems when also taking into account the interference on the feeder link, one of the few works taking into account this relevant aspect.

During the last years, a significant effort has been produced in multicast precoding techniques. Preliminary works focused on regularised channel inversion in which the users are served as a single user with an equivalent channel matrix equal to the average of the single channel matrices, [38]; in this work, the users are grouped based on their geographical locations. In [39], the authors propose a pragmatic approach in which the linear precoding and ground-based beamforming are jointly computed at the GW. The authors in [40] compute the precoding matrix by means of a block singular value decomposition (SVD). Some preliminary considerations on the challenges related to the optimal users' grouping when multicast precoding is considered are provided in [41]- [29]. The work in [42] is focused on robust multi-group multicast precoding for frame-based systems with outdated CSI; a low complexity precoder is proposed based on semi-definite relaxation and Gaussian randomisation techniques, with the numerical results showing a substantial performance improvement.
In the above context, some of the authors of this paper proposed a thorough analysis of users grouping in multicast precoding by modelling it as a clustering problem, [43]; in addition, novel clustering algorithms, both for variable and fixed cluster sizes, are proposed showing significant performance improvements (between 180% and 200%). In addition, the authors also proposed a geographical scheduling algorithm for unicast and multicast precoding, based on serving, in a specific time frame, only users that belong to the same zone within the corresponding reference beam, [44]; this algorithm showed good performance gains with respect to random user selection, *i.e.*, no scheduling at all. Finally, in [45], the same authors thoroughly assessed unicast precoding for broadband satellite systems in the context of variable beam size, *i.e.*, on-ground multi-beam coverage overlap, highlighting interesting tradeoffs between the radiation pattern value at beam edge and the achievable spectral efficiency.

In the context of precoding implemented on the feeder link, the authors of [46]- [47] extensively discuss the on-board and on-ground processing aspects for MIMO feeder links in Q/V-bands; in order to enhance the performance on the feeder link, these works focus on the proper spacing between two transmitting antennas to be properly placed at each GW, showing the benefits in terms of Carrier-to-Interference plus Noise-Ratio (CINR) and outage probability. In addition, details on the on-board architecture are reported, providing a valuable insight on this topic.

B. Paper contribution and organisation

In this paper, we move from both the well-known implementation of precoding algorithms for the forward link in unicast and multicast systems discussed in [23]- [45] and the analysis of feeder link diversity with multiple antennas per gateway in [46]- [47] by considering each gateway as a single antenna of a distributed MIMO system to which precoding is implemented, thanks to a central entity taking care of the network management and operations. In particular, the paper main contributions are the following:

- We propose a system architecture, focusing in particular on the ground control segment, detailing the operations to be performed to implement precoding on the feeder link, independently from the considered frequency band. Aspects related to the signalling information required to operate this system are also discussed.
- We provide an extensive discussion on the system performance based on numerical simulations in which the feeder link is operated in Ku, Ka, Q/V, and W bands. Such assessment provides a valuable insight on the impact of the operating frequency and, in particular, on whether precoding is actually beneficial with respect to a more traditional diversity scheme.
- We show that, unlike typical precoding implementations on the user access link, the normalisation approach providing the best performance (*i.e.*, the largest capacity) is not the Sum Power Constraint (SPC), but the Per Antenna Constraint (PAC).
- We discuss the main technical challenges, in particular related to the Channel State Information (CSI) to be provided at the transmitter side and on EHF atmospheric impairments, and provide some potential solutions to be addressed in future works.

The remainder of this paper is organised as follows: in Section II we detail the system architecture and the required signalling in order to implement precoding on the feeder link by means of a distributed set of transmitting antennas, one per gateway; in Section III, we describe the system model for linear precoding, focusing on Zero Forcing (ZF) and Minimum Mean Square Error (MMSE) approaches with different normalisations, and also provide a detailed discussion on the atmospheric impairments, one of the most critical challenges in EHF; in Section IV, we report the numerical assessment in terms of average spectral efficiency and overall system capacity when the feeder link is operated in Ku, Ka, Q/V, and W bands; Section V reports a discussion on the technical challenges for the proposed system and some potential solutions; finally, Section VI concludes this work.

C. Notation

Throughout this paper, and if not otherwise specified, the following notation is used: bold face lower case and bold face upper case characters denote column vectors and matrices, respectively. $(\cdot)^T$ denotes the matrix transposition operator. $(\cdot)^H$ denotes the matrix conjugate transposition operator. $[\cdot]$ denotes the nearest integer function. $\mathbf{a}_{i,:}$ and $\mathbf{a}_{:,i}$ denote the

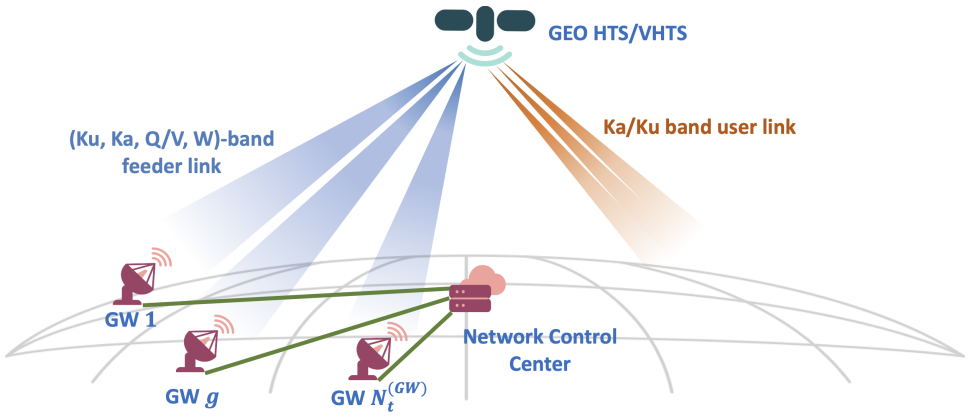

Fig. 1. Proposed system architecture for precoded EHF feeder links.

i-th row and the i-th column of matrix $\mathbf{A}$, respectively. $\angle x$ is the phase of the complex number x.

II. System Architecture

Referring to Fig. 1, we consider a HTS/VHTS GEO satellite with multi-beam coverage on both the feeder and the user links. As for the latter, it is worth mentioning that it can be implemented in Ka or Ku band, in order to exploit the available set-top boxes and antennas at the users' locations; moreover, aiming at increasing the overall capacity also on the user link, in particular for on-demand content, full frequency reuse schemes can be implemented as well. Since the paper is focused on the feeder link, aspects related to the user link will not be further discussed. As previously mentioned, in order to fully exploit the large feeder bandwidth in EHF and to cope with the large capacity requirements of future broadcasting services, full frequency reuse is implemented on the feeder link. To deal with the potentially large co-channel interference introduced in the system, linear precoding techniques are implemented at the GW side. To this aim, we assume that: i) each GW acts as a distributed antenna of a MIMO system; ii) multiple receiving antennas are co-located on-board the satellite; and iii) each beam on the feeder link is centered at the corresponding GW location.

Notably, precoding algorithms are based on the knowledge at the transmitter side of the CSI. While the detailed description of the precoding techniques and the related challenges is provided in Sections III and V, it is worth highlighting that, for the system at hand, this means that: i) the channel vector between each GW antenna and all of the on-board antennas shall be known at the on-ground control segment; and ii) a central entity in the control segment is in charge of the computation of the precoding matrix. Based on these observations, the following architecture is proposed:

- $N_t^{(GW)}$ GWs are deployed in the ground segment. Among these, during a given transmission period, $N_a^{(GW)} \leq N_t^{(GW)}$ are actually active, while the remaining $N_s^{(GW)} = N_t^{(GW)} - N_a^{(GW)}$ are spare GWs so as to exploit site diversity techniques. In this context, the Smart Gateway Diversity (SGD) concept discussed in [48], [49] can be exploited; in particular, in case of a GW malfunctioning or a deep atmospheric fade event on a specific link, the traffic provided by that GW can be re-routed. To this aim, two approaches have been proposed: i) the entire traffic of the GW is re-routed through a spare one, while the other GWs do not modify their operating behaviour; or ii) all GWs are transmitting, *i.e.*, $N_a^{(GW)} = N_t^{(GW)}$, but using less than their totally available carriers, so that when a deep fade event occurs on a link, the other $N_t^{(GW)} - 1$ GWs can take a portion of the traffic to be provided to the satellite. In the following, we assume that one of these two SGD approaches is implemented only when a malfunctioning occurs at one of the active GWs. In fact, as extensively discussed and substantiated in Section IV, the implementation of linear precoding techniques on the feeder link completely allows, with a sufficiently good estimation of the channel conditions, to deal with the detrimental impact of atmospheric events. This leads to an advantage not only in the overall system capacity compared to non-precoded solutions, but also to a less complex and reduced overhead in the ground segment when site diversity techniques are considered.
- The GEO satellite in the space segment is equipped with multi-beam antennas, which can be implemented by means of a Phased Antenna Array (PAA), a Direct Radiating Array (DRA), or an Array Fed Reflector (AFR), with a number of feeds defined by both the payload complexity and the maximum number of beams to be generated, [49]. The specific implementation is outside the scope of this paper and it will not be further discussed. In addition to the multi-beam antenna, the payload is also equipped with a Beamforming Network (BFN) in order to flexibly re-define the multi-beam coverage in order to direct the required $N_a^{(GW)}$ beams towards the active $N_a^{(GW)}$ GWs.
- The GWs are organised in a star network topology and they are managed by a Network Control Center (NCC). The NCC is the network element in charge of managing the distributed linear precoding algorithm and re-routing the traffic through the GWs that are currently active. To this aim, it shall provide the following functions: i) storage of the CSI vector for each active GW; ii)

computation of the precoding matrix based on the current $N_a^{(GW)}$ active GWs; iii) transmission of either the precoded user signals or the user signals together with the current precoding coefficients to the active GWs, depending on where in the ground control segment the signals are precoded; iv) transmission to the satellite of the list of currently active $N_a^{(GW)}$ GWs; and v) overall system synchronisation. The synchronisation among the transmitting GWs is a critical aspect. In fact, the performance of precoding is strictly related to the orthogonality among the precoding matrix columns, which defines the interfering scenario at each receiving antenna (as detailed in Section III). Thus, if two or more GWs are transmitting precoded signals that are not aligned due to a synchronisation mismatch, the performance of the precoded system will be deeply impacted. In the context of network synchronisation, many widely accepted protocols allow to properly track the network timing. Among these, two of the most common are the Network Time Protocol (NTP) and the Precision Time Protocol (PTP). In NTP, by exploiting a certain number of timekeeping servers in the network (organised in layers, with layer 0 corresponding to atomic clocks or other high-precision clocks), UTC information is provided as a response to individual requests by the network nodes; it uses a standardised User Datagram Protocol (UDP) with 64 bits and it allows to achieve a precision in the order of the picosecond. PTP, which is defined in the IEEE 1588 standard, [50], is a more advanced solution providing a finer precision compared to NTP; in particular, it is not based on the clients' requests, but it sends data that can be used to synchronise the network. The detailed assessment of the ground segment synchronisation is not the focus of this work and will not be further discussed.

There are several aspects worth to be highlighted in the above defined architecture. First of all, since the on-ground $N_t^{(GW)}$ GWs are at fixed and known locations, the beamforming coefficients to electronically steer the beams towards the active GWs can be pre-computed and stored on-board. The BFN will then be updated based on the list of active GWs to be provided by the NCC signalling information. This type of signalling is to be provided by the NCC together with a system clock reference, so as to allow the BFN to apply the correct beamforming coefficients, *i.e.*, to steer the beams towards the correct GWs for the current transmission interval; however, it is worth to mention that the list of active GWs is to be sent only when there is a modification of such elements, which might be not too often, depending on the atmospheric conditions. In addition, by implementing linear precoding techniques on the feeder link, the need to re-route the traffic towards a different GW might be limited to scenarios in which an active GW is malfunctioning, rather than due to atmospheric fading. In fact, as shown below in the system performance, with a sufficiently good quality of the CSI estimates, the precoding algorithm can take care of compensating the atmospheric impairments.

In the above network architecture there are relevant technical challenges to be tackled in order to implement the precoding techniques described in the following section, in particular related to operating in EHF and to the computation of the CSI and their signalling to the NCC. These challenges and the possible solutions are extensively discussed in Section V.

III. HTS System Model

For the considered GEO HTS system, we assume that the GWs are properly interconnected through the NCC with a star topology, as discussed above. In addition, if not otherwise specified, the following assumptions hold throughout the paper: i) the ground segment is ideal, *i.e.*, no information loss or differential delay arises in the signals exchanged among the GWs and/or the NCC; ii) linear precoding is implemented on the feeder link; iii) each GW in the ground segment acts as a single antenna of a distributed antenna system; and iv) the transparent satellite payload is equipped with a multi-beam antenna with a BFN that allows to generate $N_a^{(GW)}$ equivalent receiving antennas, each pointing to its reference on-ground active GW, based on the list of active GWs provided by the NCC. In the following, for the sake of clarity, we denote by N both the number of receiving antennas and the simultaneously active on-ground GWs, *i.e.*, $N = N_a^{(GW)}$.

Focusing on the generic i-th receiving antenna, with $i = 1, \ldots, N$, let us denote by $\mathbf{h}_{i,:} = (h_{i,1}, \ldots, h_{i,N})$ the vector of complex channel coefficients between the i-th receiving antenna and the N on-ground transmitting GWs; the single channel vector element is given by:

$$h_{i,g} = \frac{\sqrt{G_g^{(TX)}\left(\vartheta_{g,i}^{(TX)}\right) G_i^{(RX)}\left(\vartheta_{g,i}^{(RX)}\right)}}{\frac{4\pi}{\lambda}\sqrt{L_{add_{g,i}} L_{atm_{g,i}}}} \frac{e^{-\jmath\frac{2\pi}{\lambda}d_i^{(g)}}}{d_i^{(g)}} e^{-\jmath\varphi_i} \tag{1}$$

where: i) $G_g^{(TX)}\left(\vartheta_{g,i}^{(TX)}\right)$ is the transmitting antenna gain as a function of the angle between the g-th GW antenna boresight and the i-th on-board antenna direction; ii) $G_i^{(RX)}\left(\vartheta_{g,i}^{(RX)}\right)$ is the receiving antenna gain as a function of the angle between the g-th GW direction and the i-th on-board antenna boresight; iii) $d_i^{(g)}$ is the slant range between the g-th on-ground GW and the i-th on-board antenna; iv) $L_{add_{g,i}}$ models the additional system losses; v) $L_{atm_{g,i}}$ models the atmospheric losses, discussed in Section III-B; vi) $e^{-\jmath\frac{2\pi}{\lambda}d_i^{(g)}}$ models the phase offset due to the different slant range between the g-th GW and the i-th on-board antenna; and vii) $\phi_i \sim \mathcal{U}[0, 2\pi)$ is a random phase-offset at the receiving antenna equipment. In the following, we assume that the on-board antennas are co-located and that the GWs have no implementation differences, thus, $\forall i = 1, \ldots, N$: i) $\vartheta_{g,i}^{(TX)} = \vartheta_g^{(TX)}$; ii) $d_i^{(g)} = d^{(g)}$; iii) $L_{add_{g,i}} = L_{add}$, $\forall g = 1, \ldots, N$; and iv) $L_{atm_{g,i}} = L_{atm_g}$. It is worth to be mentioned that atmospheric events might also introduce a spurious phase shift between the transmitting and receiving antennas. In the considered system architecture, the receiving antennas can be assumed to be co-located and, thus, the phase shift introduced by the atmospheric events is only dependent on the transmitter index, as the atmospheric loss L_{atm_g}. In [46], the phase shift is modelled as a uniformly distributed random variable between

0 and 2π. Thus, we can assume that the phase shift due to the atmospheric fading is already included in the phase offset φ_i, which is a uniformly distributed r.v. between 0 and 2π as well. Based on this assumption, the overall channel matrix $\mathbf{H} = \left[(\mathbf{h}_{1,:})^T, \ldots, (\mathbf{h}_{N,:})^T \right]^T$ can be factorised as follows:

$$\mathbf{H} = \xi \ \mathbf{\Phi} \ \mathbf{\Omega} \ \mathbf{D} \ \mathbf{A} \tag{2}$$

where: i) $\xi = \sqrt{G^{(TX)} G^{(RX)}} / \sqrt{L_{add}} \, (4\pi/\lambda)$ is a constant equal for all GWs and receiving antennas; ii) $\mathbf{\Phi}$ is the $N \times N$ diagonal matrix of random phase-offset, *i.e.*, $[\mathbf{\Phi}]_{i,i} = e^{-\jmath \varphi_i}$; iii) $\mathbf{\Omega}$ is a $N \times N$ matrix containing the radiation pattern values of the transmitting and receiving antennas, *i.e.*, $[\mathbf{\Omega}]_{g,i} = \sqrt{\Omega^{(TX)} \left(\vartheta_g^{(TX)} \right) \Omega^{(RX)} \left(\vartheta_{g,i}^{(RX)} \right)}$, with $\Omega^{(TX)}$ and $\Omega^{(RX)}$ being the radiation pattern models for the transmitting and receiving antennas, respectively; iii) we assume that the on-board antennas are co-located and that, apart from the depointing loss discussed below, they are ideally pointed towards the satellite, thus $\Omega^{(TX)} \left(\vartheta_g^{(TX)} \right) = 1, \ \forall g = 1, \ldots, N$; iv) $\mathbf{D}$ is a $N \times N$ diagonal matrix containing the terms related to the slant range, *i.e.*, $[\mathbf{D}]_{g,g} = e^{-j \frac{2\pi}{\lambda} d^{(g)}} / d^{(g)}$; and v) $\mathbf{A}$ is the $N \times N$ diagonal matrix containing the atmospheric losses, *i.e.*, $[\mathbf{A}]_{g,g} = 1/\sqrt{L_{atm_g}}$.

With respect to the radiation pattern, we consider a Bessel antenna model at the GWs and on-board the satellite, [51]:

$$\Omega(u) = \left[\frac{(p+1)(1-T)}{(p+1)(1-T)+T} \left(2\frac{J_1(u)}{u} + \right. \right. \\ \left. \left. + \ 2^{p+1} p! \frac{J_{p+1}(u)}{(u)^{p+1}} \frac{T}{1-T} \right) \right]^2 \tag{3}$$

where p and T, with $T[\mathrm{dB}] = -10\log(1-T)^2$, are the field decay and aperture edge taper parameters, respectively, and:

$$u = u(\vartheta) = \frac{\pi d_a}{\lambda} \sin(\vartheta) \tag{4}$$

in which d_a is the equivalent antenna diameter and ϑ the off-axis angle with respect to the antenna boresight at which the pattern is computed.

Assuming a full frequency reuse scheme on the feeder link and no precoding algorithms at the GWs, the signal received at the generic i-th on-board antenna can be written as follows:

$$\begin{aligned} y_i &= \sqrt{P_t} \mathbf{h}^{(i)} \mathbf{s} + z_i \\ &= \sqrt{P_t} h_{i,i} s_i + \sqrt{P_t} \sum_{\substack{j=1 \\ j \neq i}}^{N} h_{i,j} s_j + z_i \end{aligned} \tag{5}$$

where z_i is a complex circularly-symmetric Gaussian random variable with zero-mean and variance equal to the system equivalent noise power, P_t is the transmission power, and $\mathbf{s}$ is the $N \times 1$ vector of complex transmitted symbols with unit-variance; the second formulation of eq. (5) highlights the intended and interfering components. The corresponding Signal-to-Interference plus Noise-Ratio (SINR) is given by:

$$\rho_i = \frac{P_t |h_{i,i}|^2}{P_n + P_t \sum_{\substack{j=1 \\ j \neq i}} |h_{i,j}|^2} \tag{6}$$

where P_n is the system equivalent noise power. From the above SINR equation, the rate achieved at the i-th on-board antenna, which corresponds to the rate achieved on the link with the i-th GW, can be evaluated by either the Shannon formula or from the adopted Modulation and Coding (ModCod).

A. Precoding algorithms

In order to cope with the potentially large co-channel interference due to the full frequency reuse approach, linear precoding is implemented by taking advantage of the interconnection of the on-ground GWs, which act as distributed MIMO antennas. Let us denote by $\mathbf{W}$ the $N \times N$ complex precoding matrix, built based on the CSI vectors available in the ground segment. Notably, the generic (g, i)-th element represents the weight of the signal sent from the g-th GW to the i-th on-board antenna; thus: i) the g-th row in the precoding matrix defines how the N transmitted symbols are combined at the g-th GW; and ii) the i-th column defines how the symbols intended for the i-th on-board antenna are linearly combined across the N transmitting GWs. When precoding is implemented, the received signal in eq. (5) becomes:

$$y_i = \sqrt{P_t} \mathbf{h}^{(i)} \mathbf{w}_{:,i} s_i + \sqrt{P_t} \sum_{\substack{j=1 \\ j \neq i}}^{N} \mathbf{h}^{(i)} \mathbf{w}_{:,j} s_j + z_i \tag{7}$$

With respect to the specific linear precoding algorithm, we consider the following ones:

- Zero Forcing (ZF) precoding: notably, the baseline implementation of the ZF algorithm is based on the inversion of the channel matrix $\mathbf{H}$. However, even though the channel matrix is square, it may be rank-deficient and, thus, not invertible. To circumvent this issue, we focus on the following implementation of ZF:

$$\widetilde{\mathbf{W}}_{ZF} = \left(\widetilde{\mathbf{H}}^H \widetilde{\mathbf{H}} \right)^{\dagger} \widetilde{\mathbf{H}}^H \tag{8}$$

  where $\widetilde{\mathbf{H}} \neq \mathbf{H}$ is the estimated channel matrix exploited at the ground segment to compute the precoding matrix and † denotes the Moore-Penrose pseudo-inverse matrix.
- Minimum Mean Square Error (MMSE): this is a regularised version of the ZF precoding algorithm, aimed at circumventing any issue that might arise from the ill-conditioning of the $\widetilde{\mathbf{H}}^H \widetilde{\mathbf{H}}$ matrix in eq. (8). In this case:

$$\widetilde{\mathbf{W}}_{MMSE} = \left(\widetilde{\mathbf{H}}^H \widetilde{\mathbf{H}} + \mathrm{diag}(\boldsymbol{\alpha}) \mathbf{I}_N \right)^{-1} \widetilde{\mathbf{H}}^H \tag{9}$$

  where $\boldsymbol{\alpha}$ is a vector of regularisation factors, for which the optimal value is P_n/P_t, [52].

It shall be noticed that, both with ZF and MMSE, the precoding matrix is to be properly normalised in order to take into account specific power constraints. When considering precoding on the user access link, the normalisation strategy to be adopted is defined by the power limitations of the on-board amplifiers; in particular, the constraints are to avoid operations in the non-linear regime in the on-board High Power Amplifiers (HPAs) and to ensure that the overall available transmission power is not exceeded. In the considered

feeder link scenario, the normalisation is still critical mainly for two reasons: i) the transmission power per GW shall be limited so as to ensure that the limitations defined by the radio regulations on the Earth-to-Space directions are not exceeded; and ii) the power flux density received at the on-board antennas shall not exceed a limit defined by the manufacturer of the receiving equipment. In typical SatCom systems implementing precoding, the normalisation strategy providing the best performance is the Sum Power Constraint (SPC), in which an upper bound is imposed on the total power emitted by the N GWs as follows:

$$\mathbf{W} = \frac{\widetilde{\mathbf{W}}}{\sqrt{\mathrm{tr}\left(\widetilde{\mathbf{W}}\widetilde{\mathbf{W}}^{H}\right)}} \tag{10}$$

This normalisation ensures that the total power emitted by the N GWs combined is $N \cdot P_t$ and, being a scalar factor applied to the entire precoding matrix, it also guarantees that the orthogonality among the precoding matrix columns is not modified (as discussed above, the relationships among the precoding matrix columns defines the interference scenario). However, in order to cope with the radio regulations and the on-board receiving equipment characteristics, this solution might be ineffective, since no bound is provided on a per-GW basis. Thus, the emitted power might exceed the power limitations defined at national, regional, or global level or the received power flux density might be too large for the deployed satellite. Consequently, we can consider the following normalisation strategies for the precoding matrix:

- Per Antenna Constraint (PAC), in which the upper bound is imposed at each antenna, *i.e.*, GW:

$$\mathbf{W} = \frac{1}{\sqrt{N}}\mathrm{diag}\left(\frac{1}{\| \widetilde{\mathbf{w}}_{1,:} \|}, \ldots, \frac{1}{\| \widetilde{\mathbf{w}}_{N,:} \|}\right)\widetilde{\mathbf{W}} \tag{11}$$

  It shall be noticed that, while the maximum emission level is now guaranteed at each GW, the orthogonality among the precoding matrix columns is disrupted due to the normalisation performed on each row independently from the others.
- Maximum Power Constraint (MPC), in which the aim is to preserve the orthogonality among the precoding matrix columns while not exceeding the emissions at GW level:

$$\mathbf{W} = \frac{\widetilde{\mathbf{W}}}{\sqrt{N \max_i \| \widetilde{\mathbf{w}}_{i,:} \|^2}} \tag{12}$$

  In this case, it can be easily noticed that the approach is sub-optimal, since only one GW will transmit at maximum power as per radio regulations, while the remaining $N-1$ GWs will potentially use a much lower transmission power.

In Section IV-B, we will provide a detailed comparison among the three normalisation approaches. In particular, SPC is considered as a benchmark solution, while PAC and MPC are taken into account as approaches that are actually feasible. Interestingly, we will show that SPC is not the best option in the considered scenario. These aspects will be thoroughly discussed in Section IV.

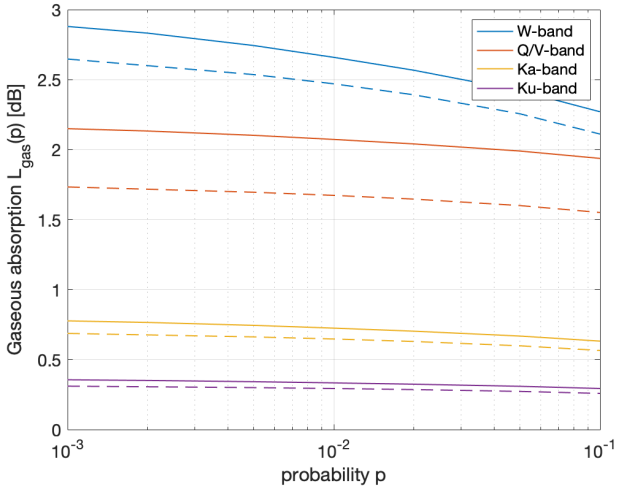

Fig. 2. Attenuation due to gaseous absorption in Cork (solid line) and Athens (dashed line) as a function of the probability of event p.

B. Atmospheric events

Notably, the attenuation due to atmospheric phenomena is non negligible in broadly used bands like Ku or Ka; in EHF, *i.e.*, the Q/V and W bands that we consider along Ka and Ku, their impact can be overwhelming. In this paper, we refer to the procedures reported in ITU-R P. 618, [53], which provides the propagation parameters and models that are needed to design both Earth-to-Space and Space-to-Earth links. In general, the sources of propagation loss that shall be considered include: gaseous absorption, cloud and fog attenuation, rain attenuation, scintillations, focusing and defocusing, the decrease in antenna gain due to wave-front incoherence, and attenuation due to sand and dust storms. However, as per ITU-R P. 618, when considering elevation angles above $10°$, a more than reasonable assumption on the feeder links of a broadcasting system, only gaseous absorption, rain and cloud attenuation, and, possibly, scintillations will be relevant. In the following, if not otherwise specified, we focus on the attenuation introduced by gas, cloud, and rain, neglecting the impact of scintillations since they are limited with respect to the other terms. The overall attenuation due to atmospheric events on the link between the g-th GW and the satellite is thus computed as:

$$L_{atm_g}(p) = L_{gas_g}(p) + L_{cloud_g}(p) + L_{rain_g}(p) \tag{13}$$

where p is the probability of the atmospheric event.

1) Gaseous absorption: This phenomenon is mainly depending on the frequency, elevation angle, altitude above the sea level, and water vapour density. The procedure to compute it is reported in ITU-R P.676, [54], in which two approximate methods and a complete one to estimate this type of absorption is provided, for frequencies up to 350 and 1000 GHz, respectively. Referring to the latter, the procedure is based on: i) approximating the atmosphere as a sequence of N_l exponentially increasing layers; ii) computing the specific attenuation $\gamma_i^{(gas)}(p)$ in dB/km and the slant path length $a_i^{(gas)}$

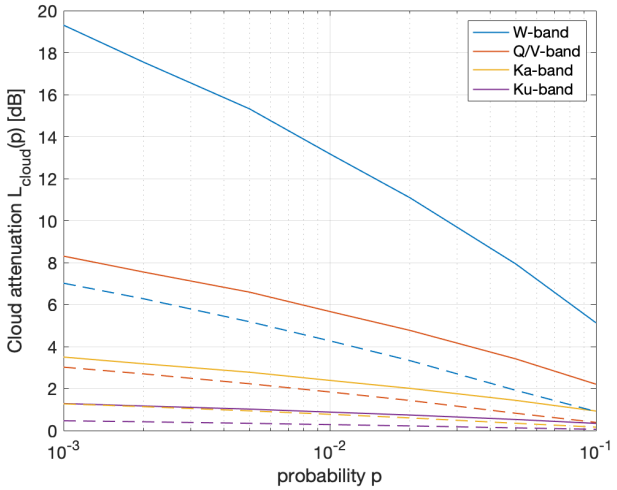

Fig. 3. Cloud attenuation in Cork (solid line) and Athens (dashed line) as a function of the probability of event p.

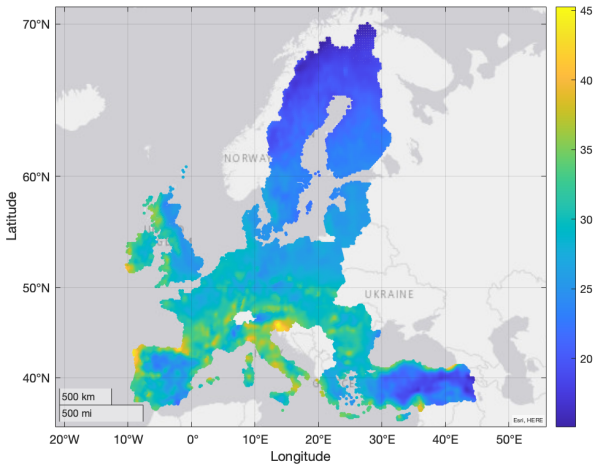

Fig. 4. Rainfall rate exceeded for 0.01% of the year, *i.e.*, $p = 10^{-4}$, as per ITU-R P. 837 version 7, [58].

for each layer; and iii) obtaining the gaseous absorption as:

$$L_{gas}(p) = \sum_{n=1}^{N_l} a_n^{(gas)} \gamma_n^{(gas)}(p) \tag{14}$$

In the absence of local data providing temperature, dry air pressure, and water vapour partial pressure profiles as a function of the height, specifications ITU-R P.835, [55], and P.836, [56], can be used to obtain, respectively, the parameters of the reference standard atmospheres and the water vapour density; please note that the latter term introduces the dependency on the probability of the atmospheric event. In order to have an idea of the impact of this term as a function of the carrier frequency, Fig. 2 shows $L_{gas}(p)$ in Ku, Ka, Q/V, and W bands for two of the GW locations considered in this work. It can be noticed that, in general, the values are limited; however, a non negligible relative variability is evident in terms of both the location and, more specifically, the operating frequency.

2) Cloud attenuation: The attenuation introduced by clouds and fog consisting of small droplets, smaller than 0.01 cm, is computed by means of the Rayleigh approximation, which is valid up to 200 GHz. For slant paths, it can be computed as reported in ITU-R P.840, [57]:

$$L_{cloud}(p) = \frac{L_{red}(p) K_l(f_c, T = 273.15)}{\sin \varepsilon} \tag{15}$$

where $L_{red}(p)$ is the total columnar content of liquid water reduced to the temperature of 273.15 K as a function of the probability p, K_l is the cloud liquid water specific attenuation coefficient, f_c is the carrier frequency, and ε is the elevation angle at the desired location. Fig. 3 shows the attenuation due to clouds and fog in two GW locations; some observations are worth being made: i) the absolute values of the cloud attenuation are significantly larger compared to the gaseous absorption, going up to 20 dB; ii) the relative variability due to the location is significant, with even 12 dB difference in W-band (in Ku-band, this effect is more limited and below 1 dB); and iii) the impact of larger probabilities is much more significant than with gaseous absorption, significantly reducing the propagation loss at 10^{-1}, in particular for larger operating frequencies. In addition, based on the prediction model in ITU-R P.840, also a significant variability in terms of the month that is being considered arises for $L_{red}(p)$ (for instance, its value can even double when moving from January to June in some locations); this aspect shall be properly considered at the network entity in charge of dealing with atmospheric events, so as to avoid any power mismatch, which could lead to service unavailability (under-estimation) or to wasting transmission power (over-estimation).

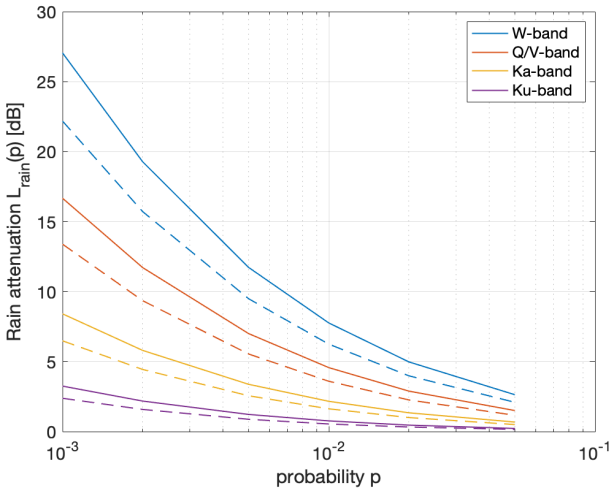

Fig. 5. Attenuation due to rain in Cork (solid line) and Athens (dashed line) as a function of the probability of event p.

3) Rain attenuation: The attenuation due to rain is computed as the product between the specific attenuation, $\gamma^{(rain)}$, and the effective path length of the wave inside the perturbation, a_e:

$$L_{rain}(p) = \gamma^{(rain)}(p) a_e \tag{16}$$

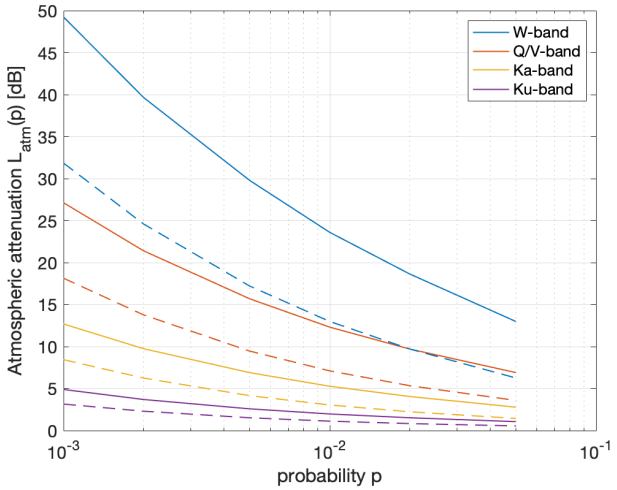

Fig. 6. Atmospheric attenuation due to gas, cloud, and rain in Cork (solid line) and Athens (dashed line) as a function of the probability of event p.

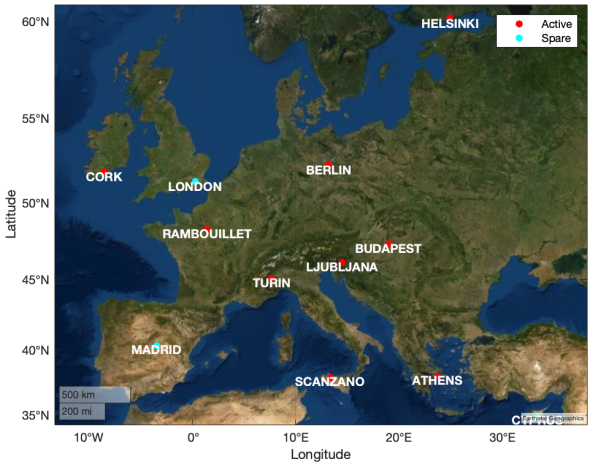

Fig. 7. Locations of the $G_a = 9$ active and $G_s = 3$ spare GWs in the considered system.

The temporal statistic, which leads to the dependency of the specific attenuation on p, is given by the cumulative probability distribution denoting the percentage of the year during which a specific value of the rainfall rate, R_p in mm/h, is exceeded. The model to compute both the specific attenuation and the slant path length is reported in ITU-R P.618. It is worth mentioning that this model is valid for frequencies up to 55 GHz. Due to the lack of other models or measurement campaigns, we will refer to this recommendation also for W-band; however, it shall be taken into account that the numerical values might be different in real scenarios, although not substantially. These aspects are clearly detailed in Section V.

The procedure to compute the terms in eq. (16) can be summarised as follows:

1) the rain height at the considered location, h_{rain}, is obtained from ITU-R P.839, [59], which also requires the Earth station height above the mean sea level. This value can be obtained from ITU-R P.1511, [60], in case it is not available;
2) the horizontal projection of the slant path length is computed (the reference geometry and the related equations are reported in [53, Section 2.2.1.1]);
3) the rainfall rate with $p = 10^{-4}$, $R_{0.01}$ exceeded for 0.01% of the year, is obtained from ITU-R P.837[1], [58]. A map reporting the values of $R_{0.01}$ in mm/h are shown in Fig. 4;
4) the specific attenuation $\gamma^{(rain)}$ is computed for $p = 10^{-4}$ as per ITU-R P.838, [61];
5) a set of correcting factors are applied to the horizontal and vertical slant path lengths allowing to compute the effective path length. Since these correcting factors are related to the probability p, this slant path is valid for $p = 10^{-4}$;
6) the rain attenuation is computed as in (16) for $p = 10^{-4}$. In case different probabilities are to be taken into account, the correcting factors are provided in [53, eq. (10)].

[1]It is worth highlighting that the current recommendation is version 7 and significant adjustments have been introduced with respect to the previous, motivated by the over-estimation of the rainfall rates in version 6.

Fig. 5 shows $L_{rain}(p)$ in Ku, Ka, Q/V, and W bands; it is worth mentioning that the model in ITU-R P.618 for the rain attenuation is valid for probabilities between 0.001% and 5%. The behaviour is similar to that observed for the cloud attenuation: i) the absolute values of rain attenuation are large, in this case also for Ka and Ku band; ii) the relative variability due to the location is more limited with respect to the cloud attenuation, but still not negligible; and iii) for increasing probabilities of the event, lower attenuations are obtained.

To conclude the analysis on the significance of the atmospheric phenomena, Fig. 6 shows the overall atmospheric attenuation in the two considered locations as per eq. (13). It can be noticed that, as expected, in W-band the attenuation due to the atmospheric phenomena is significantly larger with respect to lower frequency bands. For instance, with $p = 10^{-3}$ in Cork, $L_{atm} \approx 50$ dB in W-band, while in Q/V-band this value is approximately 26 dB, *i.e.*, almost one half; when we compare it to the Ka and Ku bands, we obtain attenuation values that are approximately 33 and 45 dB lower, respectively.

IV. Performance Assessment

In this section, we assess the numerical performance by means of Monte Carlo simulations on the feeder link with and without precoding. Both the ZF and MMSE algorithms are considered and the normalisation approach is selected so as to guarantee a maximum emitted power per GW, *i.e.*, we focus on PAC and MPC normalisations. In the following, we consider $N = 9$ active GWs and on-board receiving antennas, each with boresight direction towards the corresponding on-ground GW; the GWs' locations are provided in Fig. 7

A. Assumptions and parameters

The system design has been performed based on the parameters reported in Table I and on the considerations discussed below. It is assumed that both the GWs and the on-board

TABLE I
SYSTEM DESIGN PARAMETERS.

Parameter	**W**	**Q/V**	**Ka**	**Ku**	**units**
Carrier frequency	83.50	47.00	28.75	17.00	GHz
antenna					
diameter (GW)	3				m
efficiency (GW)	0.6	0.6	0.7	0.7	
max. gain (GW)	66.16	61.17	57.57	53.00	dBi
diameter (sat)	1	1	1.5	1.5	m
efficiency (sat)	0.6	0.6	0.7	0.7	
max. gain (sat)	56.62	51.63	51.55	46.98	dBi
additional losses					
depointing angle	0.1				deg
depointing loss (GW)	8.88	2.38	0.86	0.29	dB
depointing loss (sat)	0.80	0.25	0.21	0.07	dB
feeder loss (sat)	0.5				dB
receiver					
antenna temp. (sat)	290				K
feeder temp. (sat)	3				K
noise figure (sat)	3.0	3.0	2.5	1.8	dB
receiver temp. (sat)	288.62	288.62	225.7	148.9	K
noise temp.	547.41	547.41	484.49	407.72	K
link budget					
Target ModCod	32-APSK 5/6				
Carrier bandwidth	60				MHz
Target $\frac{E_s}{N_0}$	14.28				dB
Spectral efficiency	4.12				bit/s/Hz
roll-off	0.1				
Target $\frac{C}{N}$	13.48				dB
Target $\frac{C}{N_0}$	91.26				dBHz
$\frac{G}{T}$	27.93	23.49	23.98	20.31	dBK^{-1}
Target EIRP	100.89	81.32	63.50	55.44	dB
Required $P_t^{(GW)}$	43.61	22.53	7.45	3.40	dBW

antennas are modelled as Bessel antennas, [51], with $p = 2$ and $T = 0.9$; the radiation patterns of the on-board antennas are shown in Fig. 8. For the on-ground antennas, we assumed a fixed large antenna diameter so as to properly exploit the higher gains needed to compensate the large path loss and atmospheric attenuations; the antennas on-board the satellite are smaller in W and Q/V bands: the reduction in the diameter is compensated by the large directivity at high operating frequencies, as evident from Fig. 8, thus allowing to reduce the payload mass and cost.

In terms of additional losses, we consider the depointing loss and the feeder loss. With respect to the depointing loss, considering a 0.1° depointing, it can be noticed that in W-band the loss at the transmitter side is significantly larger compared to the other bands. This is motivated by the large directivity that the 3 meter antenna has at 83.5 GHz. At the satellite, the loss in W-band is still clearly larger than at lower frequencies, but the value is significantly lower due to the smaller antenna diameters. With respect to this type of additional loss, it is also worth mentioning that we assume the depointing loss to be affecting only the intended signal; this is motivated by focusing on a worst case scenario, in which the intended signal is further reduced with respect to the interfering ones, and by observing that the computation of the depointing loss for antennas that are not aiming at the considered GW can be non-trivial, requiring some complex geometrical considerations. Since neglecting the effect of the depointing loss on the interfering links leads to a worst case assessment, we opted for this solution.

Finally, in order to define the required transmission power, a link budget computation has been performed based on the above defined parameters and assuming: i) a probability of atmospheric event $p = 10^{-3}$, which corresponds to a service availability of 99.9% of the year; and ii) 32-APSK 5/6 as target ModCod selected from the DVB-S2X standard, [62]. In particular, the required Carrier-to-Noise spectral density-Ratio, C/N_0, is obtained as:

$$\frac{C}{N_0} = \frac{C}{N} + 10\log_{10} B_{carrier} = \frac{E_s}{N_0}\frac{1}{1+\alpha} + 10\log_{10} B_{carrier} \tag{17}$$

where α is the roll-off factor, $B_{carrier} = 60$ MHz the carrier bandwidth required by two 8K channels, and E_s/N_0 the target

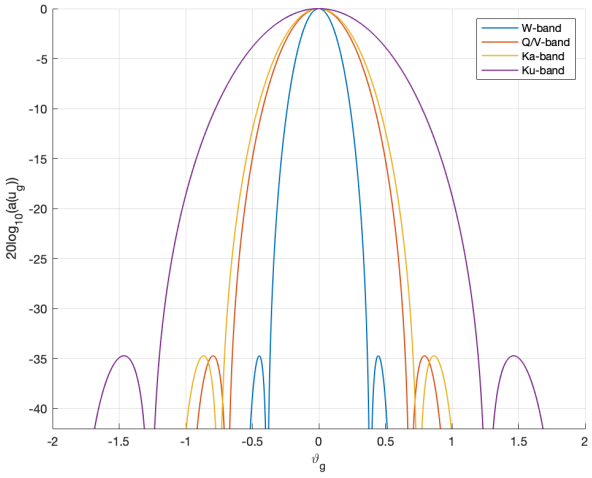

Fig. 8. Antenna radiation pattern of the on-board antennas based on the parameters in Table I and the model in eq. (3), with $p = 2$ and $T = 0.9$.

energy per symbol to noise spectral density ratio to achieve the target ModCod. From this, the required transmission power per GW is obtained as:

$$\begin{aligned} P_t^{(GW)} &= EIRP - G^{(TX)} + L_{dep}^{(TX)} \\ &= \frac{C}{N_0} + L - \frac{G}{T} - 10\log_{10}\kappa - G^{(TX)} + L_{dep}^{(TX)} \end{aligned} \tag{18}$$

where: i) $G^{(TX)}$ is the antenna gain at the GW; ii) $L_{dep}^{(TX)}$ is the depointing loss at the GW; iii) $L = L_{atm} + L_{fs}$ is the overall path loss, with L_{fs} being the free space loss, at $p = 10^{-3}$; iv) $G = G^{(RX)} - L_{dep}^{(RX)}$ is the equivalent satellite antenna gain, with $L_{dep}^{(RX)}$ being the depointing loss at the on-board antenna; v) T is the equivalent noise temperature; and vi) κ is the Boltzmann constant. It is worth highlighting that $P_t^{(GW)}$ represents the transmission power per GW when precoding is not yet taken into account. Based on the detailed discussion on the normalisation approaches for precoding, we then have one of the following scenarios: i) when SPC is the selected normalisation, the transmission power of a given GW can be above or below $P_t^{(GW)}$, but still the total power transmitted by all GWs is always equal to $N \cdot P_t^{(GW)}$, as per eq. (10); ii) when PAC is considered, the power transmitted by each GW will be exactly $P_t^{(GW)}$, as per eq. (11); iii) with MPC, see eq. (12), one GW will transmit exactly at $P_t^{(GW)}$, while all of the others will emit lower power levels.

Notably, one of the most critical challenges related to precoding is the availability of precise CSI information at the transmitter side. Since we are focusing on the performance of precoding in the presence of atmospheric events, and given the non-trivial tracking of the exact value of attenuation introduced by these, we consider that the CSI estimates available at the ground-segment are not ideal. In addition to this aspect, it shall also be highlighted that, even with an ideal estimation and tracking of the channel state, the CSI vectors that are exploited in the ground segment to compute the precoding matrix are typically outdated due to the large propagation delay. In fact, even assuming a GW at the Sub Satellite Point and not taking into account any processing time, the delay in obtaining the CSI estimates is 120 ms. In this time interval, the channel condition might vary leading to outdated CSI vectors at the GWs; however, it is also worth highlighting that we are considering a GEO HTS that is communicating with fixed on-round GWs and, thus, a limited variation of the channel conditions can be expected. To model all sources of errors on the CSI, we can assume that the channel matrix exploited in eq. (8) or eq. (9) to compute the precoding matrix is given by:

$$\widetilde{\mathbf{H}} = \mathbf{H} + \mathbf{E} \tag{19}$$

where $\mathbf{E}$ is a complex $N \times N$ matrix of CSI errors, in which the generic (i, g)-th element $e_{i,g} = |e_{i,g}|\, e^{-\jmath \angle e_{i,g}}$ is a random variable with the following amplitude and phase statistics: i) $|e_{i,g}| \sim \mathcal{N}\left(0, |h_{i,g}|^2 \sigma_a^2\right)$, in which σ_a^2 is the Cramer-Rao Bound (CRB) of the Data Aided (DA) amplitude estimation; and ii) $\angle e_{i,g} \sim \mathcal{N}\left(0, \sigma_p^2\right)$, with σ_p^2 being the CRB of the DA phase estimation. The fact that the variance on the amplitude of the error coefficient is scaled by the amplitude of the actual channel coefficient is motivated by observing that the CRB provides a normalised variance of the estimation error. As for the CRB, we can assume a Data Aided (DA) estimation strategy; in this case, the values depend on the SNR at which the estimation has been performed, which is considered a simulation parameter in the following, [63], [64]:

$$\begin{aligned} \sigma_a^2 &= \frac{1}{\ell_0}\frac{1}{SNR} \\ \sigma_p^2 &= \frac{1}{2\ell_0}\frac{1}{SNR} \end{aligned} \tag{20}$$

where ℓ_0 is the length of the data field used in DA estimation. It shall be noticed that other solutions are also available to obtain reliable estimates of the channel conditions on the feeder link. As extensively discussed in [65], channel sounding techniques can be based on the transmission of calibration signals from the satellite in the uplink band; such signals can be beacons of different types, as pseudo-noise sequences, single tone carriers, etc. In the following, we assume a DA estimation with $\ell_0 = 36$ symbols as in DVB-S2X because this is the most adopted standard for satellite communications. When other values of ℓ_0 or other technical solutions, as the beacon signal, are considered, different expressions will define the CRB for the amplitude and phase estimates of the CSI. In this context, it shall be noticed that the exact equation providing the CRB with which the CSI errors are computed does not affect the generality of the numerical results and related observations reported below.

B. Numerical results

Let us denote by $\rho_{i,n}\,(p, SNR)$ the SINR received in the n-th Monte Carlo iteration at the i-th on-board antenna, which, based on the considered system model, corresponds to the signal sent from the i-th GW; this is a function of both the probability of the atmospheric event, p, and the SNR at which

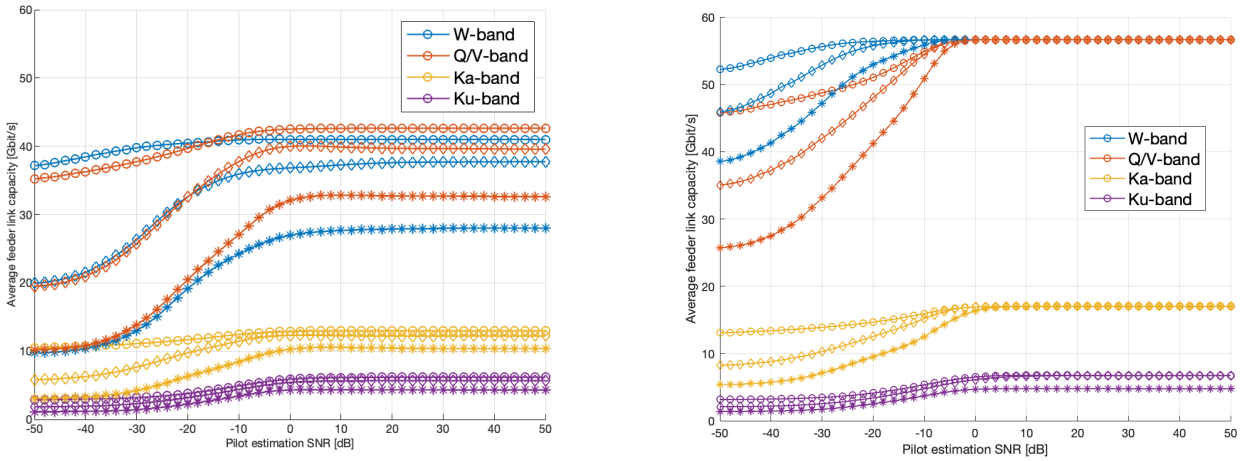

(a) $p = 10^{-3}$ (b) $p = 5 \cdot 10^{-3}$

Fig. 9. Average feeder link capacity with PAC (circle), SPC (diamond), and MPC (asterisk) with MMSE precoding as a function of the pilot estimation SNR.

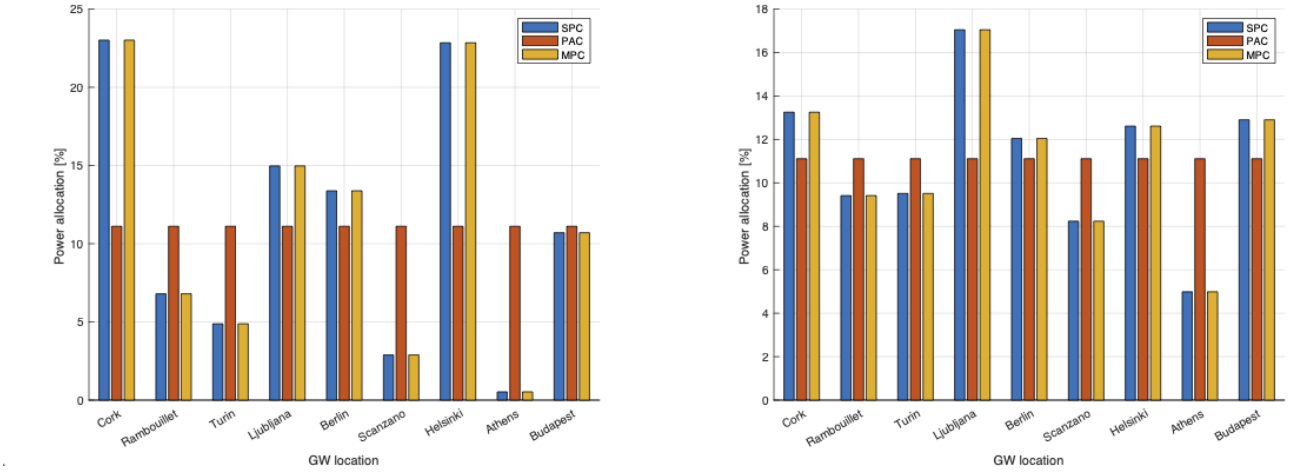

(a) W-band (b) Ka-band

Fig. 10. Percentage of power allocated per GW with SPC, PAC, and MPC in W-band (left) and Ka-band (right), $p = 10^{-3}$ (99.9% availability).

the CSI estimates are obtained, SNR. From this, we can obtain the corresponding spectral efficiency as:

$$\eta_{i,n}\left(p, SNR\right) = f\left(\rho_{i,n}\left(p, SNR\right)\right) \tag{21}$$

where $f(\cdot)$ represents the function providing the spectral efficiency as a function of the received SINR for DVB-S2X ModCods. Clearly, the Shannon formula or other standards with different spectral efficiency and threshold values can be adopted, without affecting the generality of our analysis. The first Key Performance Indicator (KPI) that we discuss is the average spectral efficiency on the feeder link as a function of (p, SNR), obtained by averaging over all GWs and Monte Carlo iterations:

$$\overline{\eta}\left(p, SNR\right) = \mathbb{E}_{i,n}\left\{\eta_{i,n}\left(p, SNR\right)\right\} \tag{22}$$

The average spectral efficiency is evaluated with and without precoding; in the latter case, both the ZF and MMSE approaches are considered with MPC and PAC normalisations.

1) Precoding normalisations: The first analysis that we report is the comparison between the three different normalisation methods detailed in Section III, *i.e.*, SPC, PAC, and MPC. Figure 9 shows the overall capacity on the feeder link based on the bandwidth allocations, with guard bands, in Table IV with the three normalisations, $p = 10^{-3}$ (left), *i.e.*, 99.9% availability, and $p = 5 \cdot 10^{-3}$ (right), *i.e.*, 99.5% availability. It can be noticed that the performance with SPC is significantly worse than PAC at low atmospheric event probabilities, while for increasing values of the probability the performance tend to be the same with a sufficiently good SNR for pilot estimation. This behaviour needed a detailed analysis, since SPC is usually the best option in user link precoding. To this aim, we can analyse the power allocations with PAC, SPC, and MPC, shown in Figure 10 for W and Ka bands, respectively. With SPC (and MPC, which is identical in the percentage of power allocated to the transmitters, but not in the total amount of power), the precoder tries to give a much larger fraction of

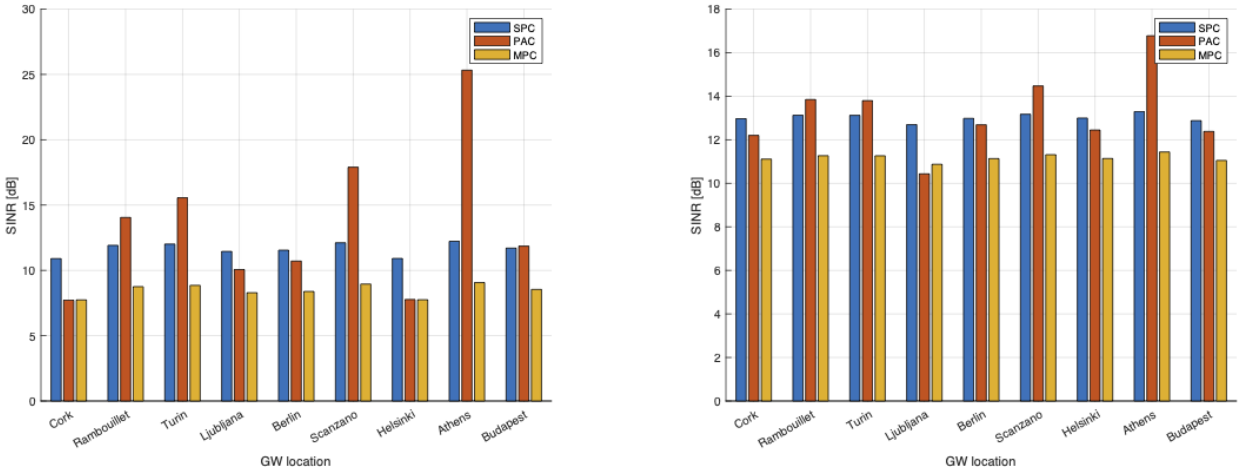

(a) W-band (b) Ka-band

Fig. 11. Average SINR per GW with SPC, PAC, and MPC in W-band (left) and Ka-band (right), $p = 10^{-3}$ (99.9% availability).

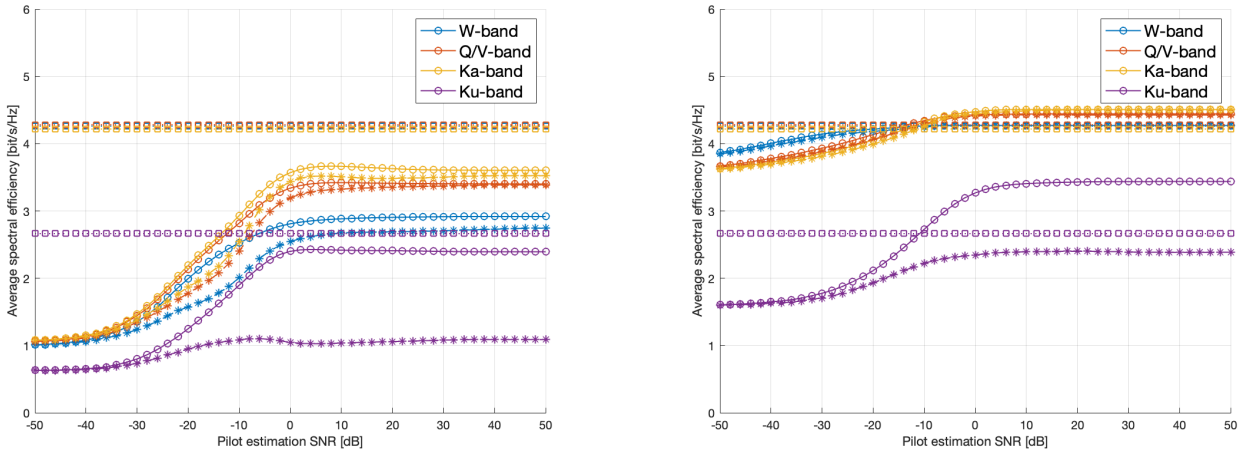

(a) MPC (b) PAC

Fig. 12. Average spectral efficiency with MMSE (circle), ZF (star), and without precoding (square) as a function of the pilot estimation SNR with MPC (left) and PAC (right) normalisation, $p = 10^{-3}$ (99.9% availability).

TABLE II
RADIATION PATTERN VALUES AT THE ON-BOARD ANTENNAS FOR EACH GW: W-BAND.

	Cork	Rambouillet	Turin	Ljubljana	Berlin	Scanzano	Helsinki	Athens	Budapest
Cork	0,00	-57,36	-50,92	-61,51	-59,47	-57,90	-86,00	-62,60	-57,39
Rambouillet	-57,36	0,00	-61,87	-55,04	-51,79	-58,86	-55,63	-74,77	-57,17
Turin	-50,92	-61,87	0,00	-46,30	-48,44	-54,17	-53,24	-54,44	-53,66
Ljubljana	-61,51	-55,04	-46,30	0,00	-47,11	-49,63	-50,06	-51,62	-42,58
Berlin	-59,47	-51,79	-48,44	-47,11	0,00	-72,70	-75,51	-56,09	-45,65
Scanzano	-57,90	-58,86	-54,17	-49,63	-72,70	0,00	-54,75	-49,27	-48,93
Helsinki	-86,00	-55,63	-53,24	-50,06	-75,51	-54,75	0,00	-68,44	-49,79
Athens	-62,60	-74,77	-54,44	-51,62	-56,09	-49,27	-68,44	0,00	-86,54
Budapest	-57,39	-57,17	-53,66	-42,58	-45,65	-48,93	-49,79	-86,54	0,00

power to signals which are sent on links experiencing deeper atmospheric fades. In more typical implementations, in fact, the off-axis angles at which the receiver sees the different transmitting antennas are smaller, giving to the precoder more flexibility in allocating the power so as to truly exploit the reception of signals of similar power levels from multiple antennas. In this case, the off-axis angles are larger and, consequently, the precoder tries to overcome this limitation by

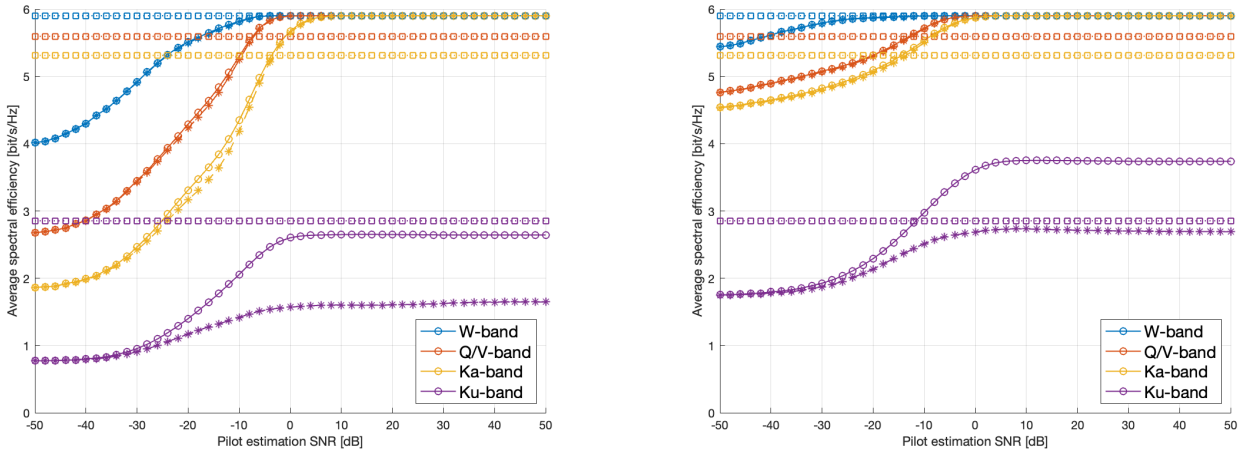

(a) MPC (b) PAC

Fig. 13. Average spectral efficiency with MMSE (circle), ZF (star), and without precoding (square) as a function of the pilot estimation SNR with MPC (left) and PAC (right) normalisation, $p = 5 \cdot 10^{-3}$ (99.5% availability).

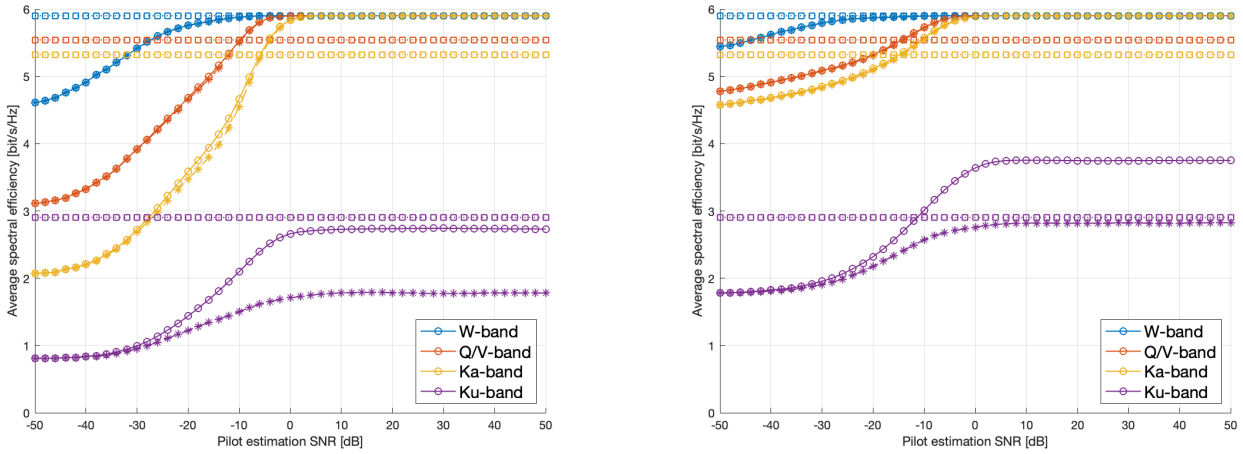

(a) MPC (b) PAC

Fig. 14. Average spectral efficiency with MMSE (circle), ZF (star), and without precoding (square) as a function of the pilot estimation SNR with MPC (left) and PAC (right) normalisation, $p = 10^{-2}$ (99% availability).

behaving similarly to a water-filling algorithm. The resulting SINR levels at the receiving antennas (each directed towards a specific GW) are shown in Figure 11. Comparing SPC and PAC, we can notice that the SINR levels for the GWs in which the deepest fades are experienced have similar values: the SPC is usually slightly larger by $2-3$ dB at most, but it is actually capable of overcoming the atmospheric events. However, this results in a significant penalisation for signals that experience lower attenuations: in fact, the total amount of transmission power is fixed and, in order to compensate the largest fades, SPC deeply penalises other signals. This is not happening with PAC because the same transmission power is allocated to all signals. As a consequence, while for the GWs is bad atmospheric conditions the performance are close between SPC and PAC, for the other GWs the PAC normalisation results in a significantly larger SINR, *i.e.*, capacity. On the other hand, this also introduces a fairness issue in the system, which shall in any case be taken into account. It is worth highlighting that this effect is evident on the feeder link scenario considered in this work because, as we highlighted above, the amount of power received at a specific on-board antenna that arrives from the other transmitting antennas is limited. Thus, this effect is particularly evident in W and Q/V bands. The above analysis was performed with ideal CSI estimates. When non ideal CSI estimates are considered, the gap between PAC and SPC is more significant at low estimation SNRs. This can be motivated by observing that PAC *a priori* disrupts the orthogonality among the precoding matrix columns while ensuring that all signals are transmitted at the same power level. On the other hand, SPC does not modify the orthogonality. Consequently, the impact of non-ideal CSI is more relevant with SPC because the errors on the channel matrix used to compute the precoding matrix actually lead to significantly mismatched power allocations. On the

TABLE III
RADIATION PATTERN VALUES AT THE ON-BOARD ANTENNAS FOR EACH GW: KU-BAND.

	Cork	Rambouillet	Turin	Ljubljana	Berlin	Scanzano	Helsinki	Athens	Budapest
Cork	0,00	-14,26	-37,66	-56,17	-47,44	-45,60	-46,97	-48,05	-54,79
Rambouillet	-14,26	0,00	-8,15	-34,73	-38,55	-45,93	-50,47	-64,21	-45,95
Turin	-37,66	-8,15	0,00	-11,09	-15,83	-21,75	-44,85	-52,36	-39,75
Ljubljana	-56,17	-34,73	-11,09	0,00	-5,39	-15,43	-37,17	-36,12	-4,13
Berlin	-47,44	-38,55	-15,83	-5,39	0,00	-34,81	-23,46	-44,94	-10,56
Scanzano	-45,60	-45,93	-21,75	-15,43	-34,81	0,00	-53,75	-36,05	-37,72
Helsinki	-46,97	-50,47	-44,85	-37,17	-23,46	-53,75	0,00	-45,70	-20,48
Athens	-48,05	-64,21	-52,36	-36,12	-44,94	-36,05	-45,70	0,00	-47,41
Budapest	-54,79	-45,95	-39,75	-4,13	-10,56	-37,72	-20,48	-47,41	0,00

other hand, PAC introduces a sort of controlled orthogonality loss, thus reducing the impact that wrong CSI vectors have on the precoding performance. In the following, we thus focus on PAC and MPC so as to: i) consider normalisations that upper-bound the transmission power per antenna, so as to satisfy any constraint in terms of radio regulations or received power flux density at the on-board antennas; and ii) show the performance with the best and worst performing approach, providing the actual bound for precoding on the feeder link.

2) Upper-bounded power per antenna: Based on the above considerations, in the following we only consider PAC and MPC normalisations, since they guarantee that the transmission power per GW is upper-bounded. Figures from 12 to 14 show the average spectral efficiency in eq. (22) with probability of atmospheric event equal to 10^{-3} (0.1%), $5{\cdot}10^{-3}$ (0.5%), and 10^{-2} (1%), *i.e.*, the service availability is equal to 99.9%, 99.5%, and 99%; the SNR at which the channel coefficients are estimated ranges from -50 to 50 dB, so as to have a clear insight of the impact of this parameter. First focusing on the precoding algorithms and normalisations, the following general trends can be identified:

- MMSE precoding is always performing at least as good as ZF, as expected from well-known results in the context of MIMO systems and algorithms. More specifically, they provide the same performance in the majority of scenarios, with the only exception being the spectral efficiency in Ku-band and, in a significantly more limited way, in Ka-band, with MMSE being much better;
- the PAC normalisation is always outperforming MPC. As discussed above, MPC is motivated by the intention to keep unaltered the orthogonalities in the precoding matrix columns, which directly define the ability to maximise the intended signal and limit the interfering ones as evident from eq. (7). However, this normalisation significantly limits the intended signal power, *i.e.*, the SNR, because only one GW will be allowed to transmit at full power, in particular the GW with index $g = \arg\max_i \| \widetilde{\mathbf{w}}_{i,:} \|^2$: the remaining $N-1$ GWs can transmit at, eventually much, lower power levels. Thus, although with PAC the orthogonality among the precoding matrix columns is disrupted, there is a significantly more impacting benefit in always transmitting at maximum power. This is particularly evident in Ku-band, in which MPC does not achieve the rates obtained without precoding;
- in terms of the non ideality of the CSI, independently from the considered operating frequency, we can notice that the precoded performance reaches its maximum with SNR in the order of $15-20$ dB. More specifically, when $SNR > 20$ dB, an asymptotic value is always achieved; the only exception to this behaviour can be noticed in W-band, as discussed below.

Focusing on the impact of precoding as a function of the operating frequency, some very useful and interesting trends can be observed in addition to those above; in particular, by observing Figure 15, in which the relative gain of the precoded system compared to the non-precoded one with full frequency reuse is shown, the following trends can be highlighted:

- in Ku-band, when MMSE precoding with PAC is considered, the benefit is evident; in particular, the relative gain with respect to the non precoded system is in the order of 30%, when the asymptotic optimum of MMSE-PAC is achieved. With MMSE-MPC, as already mentioned the power normalisation is negatively impacting the performance and a performance loss is experienced;
- in Ka and Q/V bands, the benefit introduced by precoding becomes less evident, but still present. In particular, in the former case the relative gain is included between 6% and 11%, while in the latter it is between 3.6% and 6.5% with MMSE-PAC, while for MMSE-MPC a limited asymptotic gain is achieved with larger probabilities of the atmospheric event, *i.e.*, when more transmission power is allocated compared to that required by the atmospheric event: this is in line with the previous considerations on the SNR loss with this precoding solution;
- in W-band, no benefit is introduced by precoding, since when the asymptotic maximum value is achieved for MMSE-PAC, the same rate as in the non-precoded system is achieved. The motivation for this, perhaps non intuitive, behaviour can be found in the antenna radiation pattern. This aspect can be already seen in Fig. 8, showing the antenna radiation pattern as a function of the frequency.

With respect to the latter aspect, Tables II and III report the radiation pattern values of the on-board antennas towards each on-ground GW, for W and Ku bands, respectively; on each row, we thus have the radiation pattern values towards each GW of an on-board antenna aiming at the GW of that row

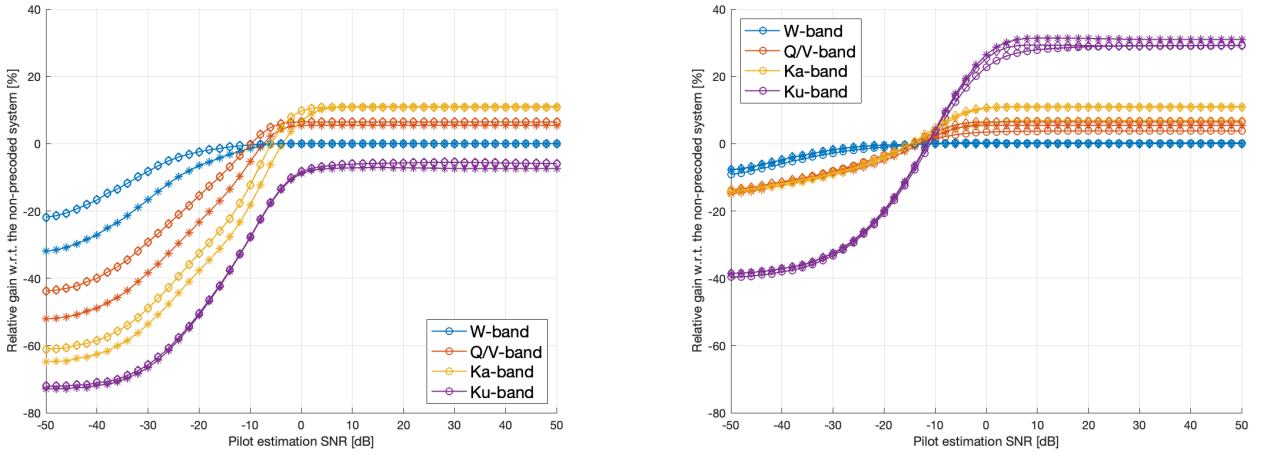

(a) MPC (b) PAC

Fig. 15. Relative gain obtained with precoding compared to the non-precoded system with MMSE precoding, MPC (left) and PAC (right) normalisations, as a function of the atmospheric event probability: $p = 10^{-3}$ (circle), $p = 5 \cdot 10^{-3}$ (star), and $p = 10^{-2}$ (diamond).

TABLE IV
SYSTEM CAPACITY EVALUATION.

Parameter	W	Q/V	Ka	Ku	units
Feeder link bandwidth	10	10	3	1.9	GHz
Carriers per GW	160	160	48	30	

(diagonal element). It can be noticed that GWs that in Ku-band can actually benefit from the cooperative transmission achieved with precoding (for instance, Rambouillet and Turin or Budapest and Ljubljana, with radiation patterns in the order of -8 and -4 dB, respectively), are significantly more separated in W-band (-61 and -42 dB). Based on these observations, it can be concluded that, when the on-ground GWs are sufficiently geographically separated, the benefit in implementing interference cancellation techniques decreases with increasing operating frequencies at the point that, in W-band, no benefit is obtained. This discussion, although substantiated by means of a specific geographical distribution of the GWs and system-level assumptions, is general. Thus, in W-band the significantly directive radiation patterns already provide sufficient interference rejection to operate with a full frequency reuse scheme; in case further enhanced capacities might be needed, more complex and advanced solutions encompassing multiple antennas per GW, with proper spatial separation, can be implemented, as proposed in [46]- [47].

To conclude the numerical assessment of the proposed system, in figures from 16 to 18 we provide the overall capacity on the feeder link based on the bandwidth allocations in Table IV, in which proper guard bands have been included as well. We are now focusing on MMSE-PAC compared to the non precoded system, since it has been shown to be the best solution. Clearly, the general trends are the same as in the average spectral efficiency discussed above, since the curve for each band is multiplied by the number of carriers per GW. However, when observing the behaviour for a varying

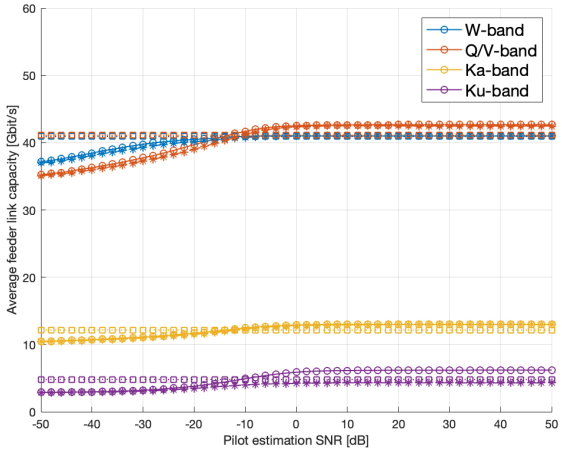

Fig. 16. Average feeder link capacity with MMSE-PAC (circle) and without precoding (square) as a function of the pilot estimation SNR, $p = 10^{-3}$ (99.9% availability).

operating frequency, we can notice that the advantage in exploiting EHF allocations becomes significant:

- Ku-band systems with MMSE-PAC precoding can achieve an overall feeder link capacity of 6.18, 6.72, and 6.74 Gbps for a service availability of 99.9%, 99.5%, and 99%, respectively. When moving to Q/V-band, the achievable capacity becomes 42.48, 56.65, and 56.65 Gbps in the same cases, yielding a relative gain of 587.4%, 743.0%, and 742.7%, respectively. In W-band, it can be noticed that the only different gain is obtained with a 99.9% availability, since the maximum achievable capacity is 41.1 Gbps (in all of the other cases, the same asymptotic value is obtained for W and Q/V bands), providing a relative gain in the order of 565%;
- when considering Ka-band systems, the achievable capacity is 12.98, 16.99, and 16.99 Gbps for a service

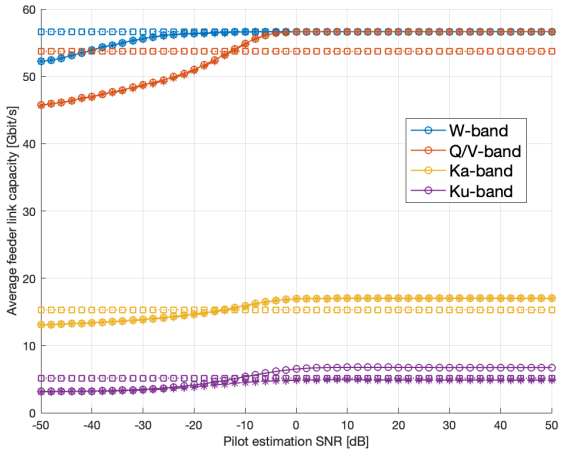

Fig. 17. Average feeder link capacity with MMSE-PAC (circle) and without precoding (square) as a function of the pilot estimation SNR, $p = 5 \cdot 10^{-3}$ (99.5% availability).

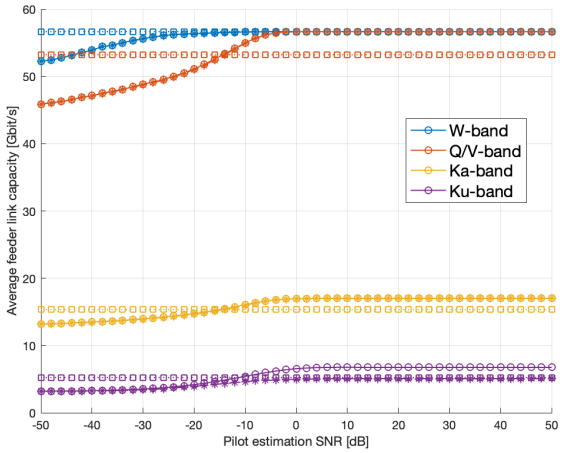

Fig. 18. Average feeder link capacity with MMSE-PAC (circle) and without precoding (square) as a function of the pilot estimation SNR, $p = 10^{-2}$ (99% availability).

availability of 99.9%, 99.5%, and 99%, respectively. This leads to the following corresponding relative gains in EHF: i) in Q/V-band, we have a 227.3%, 233.4%, and 233.4% improvement; ii) in W-band, the gain is in the order of 216.6%, 233.4%, and 233.4%.

It is worthwhile highlighting again that the huge gains obtained in Q/V-band assume the implementation of MMSE-PAC, even though the performance without precoding is quite close thanks again to the very directive antenna radiation patterns on-board the satellite. In W-band, we are taking the asymptotic MMSE-PAC performance, which is that obtained without precoding: thus, the above gains can be obtained by simply exploiting the EHF frequency range without any additional complexity, at least from the interference management point of view. Clearly, other challenges arise in exploiting such large operating frequencies, as discussed in the next section.

3) Comparison with FR3: To provide further details on the numerical assessment, we now provide a comparison between the proposed precoded system and a system in which precoding is not implemented based on a frequency reuse scheme with 3 colours. Since in this paper we focused on a single polarisation, we assume that also in the FR3 case the overall bandwidth is split into 3 equal chunks on the same polarisation. As for the allocation of the spectral resources to the different GWs, the following holds: i) bandwidth 1 allocated to Cork, Ljubljana, and Berlin; ii) bandwidth 2 allocated to Rambouillet, Scanzano, and Helsinki; and iii) bandwidth 3 allocated to Turin, Athens, and Budapest. Since the available bandwidth per GW is one third compared to the precoded system, the transmission power is also one third of $P_t^{(GW)}$, so as to ensure that the same EIRP density is emitted. Table V reports the performance in terms of both the average spectral efficiency and the average feeder link capacity. It can be noticed that the average spectral efficiency is quite similar to that obtained with the precoded system; this is reasonable, since we already observed that thanks to the geographical separation of the GWs interference is limited and here we are further reducing it with frequency reuse. However, the overall capacity on the feeder link is significantly decreased, since each GW now has approximately one third of the carriers. Thus, full frequency reuse is still the best option, with or without precoding.

TABLE V
FR3 PERFORMANCE WITHOUT PRECODING.

Parameter	W	Q/V	Ka	Ku
$p = 10^{-3}$				
Carriers per GW	52	52	16	10
Average spectral efficiency [bit/s/Hz]	4.43	4.49	4.39	3.86
Average capacity [Gbit/s]	13.82	14.01	4.21	2.32
$p = 5 \cdot 10^{-3}$				
Average spectral efficiency [bit/s/Hz]	5.09	5.09	5.74	4.64
Average capacity [Gbit/s]	18.41	18.41	5.51	2.78
$p = 10^{-2}$				
Average spectral efficiency [bit/s/Hz]	5.09	5.09	5.85	4.89
Average capacity [Gbit/s]	18.41	18.41	5.62	2.93

4) Performance with other GWs: To conclude the numerical assessment, we provide the performance results obtained with GWs in different locations. In particular, compared to the previous locations, in the following we assume that Athens, Scanzano, and Rambouillet are not active and replaced by the GWs in Madrid, Cyprus, and London. Figure 19 shows the relative gain obtained in this case. It can be noticed that the general trends and asymptotic gains discussed above still hold. The main difference is related to the increased sensitivity to the non-idealities in the CSI knowledge, with a larger value of the estimation SNR that is required to achieve the average spectral efficiency values for the previous scenario. Clearly, the specific asymptotic values or the required estimation SNRs will differ from one scenario to another, in terms of GWs locations, but the generality of the conclusions of this paper holds.

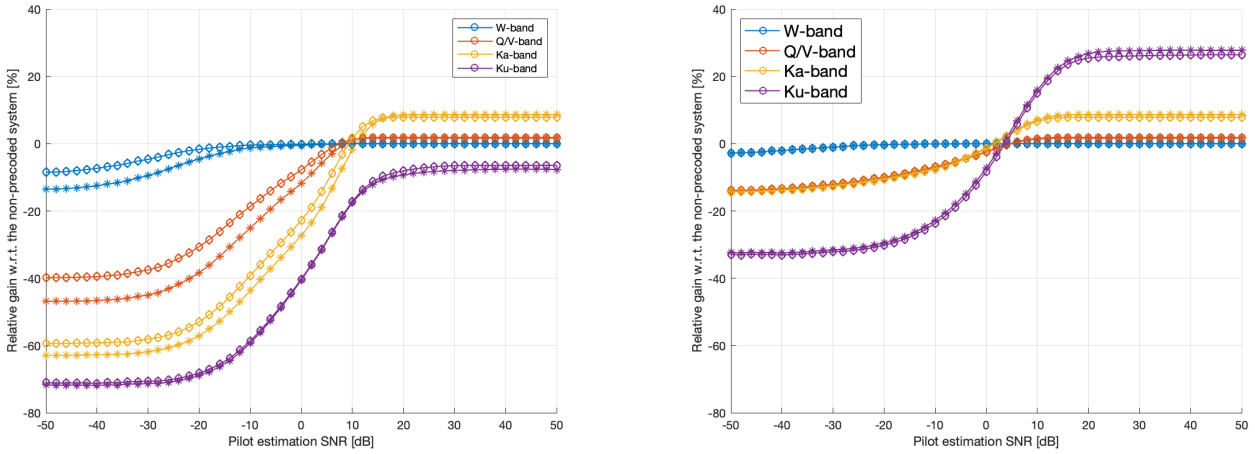

(a) MPC (b) PAC

Fig. 19. Relative gain obtained with precoding compared to the non-precoded system with MMSE precoding, MPC (left) and PAC (right) normalisations, as a function of the atmospheric event probability: $p = 10^{-3}$ (circle), $p = 5 \cdot 10^{-3}$ (star), and $p = 10^{-2}$ (diamond). Spare GWs replacing Athens, Scanzano, and Rambouillet.

V. Technical Challenges and Potential Solutions

One of the most critical challenges to be coped with is related to the availability of the CSI estimates at the NCC, which are required to compute the precoding matrix. In the proposed system, the channel vector to be estimated is that related to the uplink between a generic GW and the satellite receiving antennas, which is non-trivial due to the Frequency Division Duplexing (FDD) implemented on the feeder link, preventing the possibility to exploit the channel reciprocity. In this context, the following solutions can be proposed:

- the satellite payload might be equipped with additional components and software so as to be able to estimate the channel based on dedicated pilot fields inserted in the frames sent from the GWs. However, this approach is likely to lead to an increase in the payload complexity and mass, which is often undesirable in terms of satellite manufacturing and management costs;
- to avoid any increased on-board complexity, the channel estimates might actually be computed on-ground. To this aim, it is worth to highlight that the GWs are fixed and at known locations, thus leaving to the atmospheric impairments the only source of misalignment compared to the *a priori* known clear-sky channel conditions. Thus, it would be sufficient at the ground segment to estimate the amount of atmospheric fading currently present on each feeder link. To this aim, the system can rely on the return link information, if any, to estimate the CSI at the GWs, which then forward such information to the NCC; the NCC can then apply proper correction factors, to take into account the different uplink and downlink feeder frequencies, and compute the precoding matrix. More specifically, it is worth to highlight that, typically, both the GWs and the user terminals are on the same, extremely large, coverage area. Since all of the users' set-top boxes already estimate the channel quality, such information might be forwarded back to the NCC in order to provide accurate real-time estimates of the atmospheric conditions over the entire coverage area. This would not only provide the possibility to refine the CSI estimation, but also to predict the evolution of the atmospheric conditions so as to enhance the system reliability and promptness in responding to them. To provide the channel estimates from each user terminal to the NCC, it shall be mentioned that most of the set-top boxes today are connected to the Internet; thus, there would be no need to congestion the traffic on the return link, since high-speed terrestrial connections, *e.g.*, fiber optics, can be used to this aim.

In addition, as mentioned in Section IV, other solutions are also available to obtain reliable estimates of the channel conditions on the feeder link. For instance, channel sounding techniques can be implemented based on the transmission of calibration signals from the satellite in the uplink band that can be beacons of different types. The analysis reported in this work is based on a pilot approach with non-idealities modelled through the CRB for DA estimation, but the same approach can be used for other values of the number of pilot symbols or other signalling choices, by modifying the CRB accordingly.

Concerning physical layer (PHY) issues, the adoption of distortion and phase-noise resilient transmission waveforms would definitely improve the precoding performance. The development of suitable transmission and channel coding formats for multi-gigabit satellite applications is still under investigation, because the theoretical performance improvement yielded by new waveforms is often in trade-off with the hardware feasibility of the modem chain, as shown, for instance, in [12].

Finally, it should be noticed that the analysis reported in this paper has been carried out on the basis of approximated rain fading models, commonly accepted by the satellite community. However, a more precise picture of the precoding system behaviour in EHF-based HTSs will be drawn only if precise data about channel measurement campaigns will be available. So far, the campaign is partial and only related to

the Q/V-band, while no experimental data-set concerning W-band propagation is available yet.

VI. Conclusion

In this work, we focused on the implementation of linear precoding algorithms on the feeder link of a future broadcast satellite system operating with full frequency reuse. More specifically: i) we proposed a detailed system architecture, detailing the operations that the different control segment elements (GWs and NCC) have to perform in order to provide such service and also providing an insight on the type of signalling that is needed; ii) we showed that, due to the peculiarities of the feeder link geometry, the SPC normalisation that does not limit the power per antenna (typically the best in user access link precoding) is not the most suitable choice, while PAC, in which all transmitters emit the same power, provides the best capacity; iii) we extensively discussed the system performance for a varying operating frequency (Ku, Ka, Q/V, W) and with MMSE and ZF precoding in which both PAC and MPC normalisations are applied; iv) we provided a comparison with non-precoded systems implementing a frequency reuse scheme with 3 colours, showing that, due to the limited bandwidth per GW, solutions based on full frequency reuse and interference management with MMSE-PAC are still the best option; and v) we detailed the main technical challenges, in particular related to the CSI computation and accuracy and on PHY aspects. In general, MMSE-PAC solutions are those providing the largest capacity; in this context, it has been shown that precoding can provide significant benefits in terms of average spectral efficiency and system capacity in particular in low (Ku, Ka) frequency bands and, in part, also in Q/V-band. As for W-band systems, the significantly directive radiation patterns on-board the satellite already provide an effective interference rejection, thus making it possible to exploit EHF allocations in full frequency reuse without the need for advanced techniques as precoding. Clearly, aiming at a further increased capacity, more complex solutions, for instance based on multiple antennas per GW as already proposed in the literature, can be envisaged. To further substantiate the generality of the results and conclusions of this work, the performance with a different combination of active GWs was also reported, showing the same trends as those extensively discussed before.

VII. Acknowledgments

The research activities presented in this paper fall within the field of interest of the IEEE AESS technical panel on Glue Technologies for Space Systems.

References

[1] C. W. Paper. (2020) Cisco annual internet report (2018–2023),.

[2] V. Mignone, M. A. Vazquez-Castro, and T. Stockhammer, "The Future of Satellite TV: The Wide Range of Applications of the DVB-S2 Standard and Perspectives," *Proceedings of the IEEE*, vol. 99, no. 11, pp. 1905–1921, 2011.

[3] S. Dulac and J. Godwin, "Satellite Direct-to-Home," *Proceedings of the IEEE*, vol. 94, no. 1, pp. 158–172, 2006.

[4] C. Sacchi, T. Rossi, M. Murroni, and M. Ruggieri, "Extremely High Frequency (EHF) Bands for Future Broadcast Satellite Services: Opportunities and Challenges," *IEEE Transactions on Broadcasting*, vol. 65, no. 3, pp. 609–626, 2019.

[5] C. Stallo and C. Sacchi, "Link performance analysis of multi-user detection techniques for W-band multi-beam satellites," in *2016 IEEE Aerospace Conference*, 2016, pp. 1–9.

[6] A. J. Roumeliotis, C. I. Kourogiorgas, and A. D. Panagopoulos, "Dynamic capacity allocation in smart gateway high throughput satellite systems using matching theory," *IEEE Systems Journal*, vol. 13, no. 2, pp. 2001–2009, 2019.

[7] ——, "Optimal dynamic capacity allocation for high throughput satellite communications systems," *IEEE Wireless Communications Letters*, vol. 8, no. 2, pp. 596–599, 2019.

[8] O. B. Usman and A. Knopp, "Digital predistortion in high throughput satellites: Architectures and performance," *IEEE Access*, vol. 9, pp. 42 291–42 304, 2021.

[9] G. Giambene, S. Kota, and P. Pillai, "Satellite-5g integration: A network perspective," *IEEE Network*, vol. 32, no. 5, pp. 25–31, 2018.

[10] C. Sacchi, G. Gera, and C. S. Regazzoni, "W-band physical layer design issues in the context of the DAVID-DCE experiment," *Int. J. Satellite Commun. Netw.*, vol. 22, no. 2, pp. 193–215, 2004.

[11] T. Rossi, M. De Sanctis, and F. Maggio, "Evaluation of Outage Probability for Satellite Systems Exploiting Smart Gateway Configurations," *IEEE Communications Letters*, vol. 21, no. 7, pp. 1541–1544, 2017.

[12] C. Sacchi, T. Rossi, M. Ruggieri, and F. Granelli, "Efficient waveform design for high-bit-rate w-band satellite transmissions," *IEEE Transactions on Aerospace and Electronic Systems*, vol. 47, no. 2, pp. 974–995, 2011.

[13] C. Sacchi, T. Rossi, M. Menapace, and F. Granelli, "Utilization of uwb transmission techniques for broadband satellite connections operating in w-band," in *2008 IEEE Globecom Workshops*, 2008, pp. 1–6.

[14] M. De Sanctis, E. Cianca, T. Rossi, C. Sacchi, L. Mucchi, and R. Prasad, "Waveform design solutions for ehf broadband satellite communications," *IEEE Communications Magazine*, vol. 53, no. 3, pp. 18–23, 2015.

[15] S. Mukherjee, M. De Sanctis, T. Rossi, E. Cianca, M. Ruggieri, and R. Prasad, "On the optimization of DVB-S2 links in EHF bands," in *2010 IEEE Aerospace Conference*, 2010, pp. 1–11.

[16] A. Fantinato, N. Conci, T. Rossi, and C. Sacchi, "Performance analysis of w-band satellite hdtv broadcasting," in *2011 Aerospace Conference*, 2011, pp. 1–12.

[17] M. Ruggieri, S. De Fina, M. Pratesi, E. Saggese, and C. Bonifazi, "The W-band data collection experiment of the DAVID mission," *IEEE Transactions on Aerospace and Electronic Systems*, vol. 38, no. 4, pp. 1377–1387, 2002.

[18] M. Lucente, T. Rossi, A. Jebril, M. Ruggieri, S. Pulitano, A. Iera, A. Molinaro, C. Sacchi, and L. Zuliani, "Experimental Missions in W-Band: A Small LEO Satellite Approach," *IEEE Systems Journal*, vol. 2, no. 1, pp. 90–103, 2008.

[19] T. Rossi, M. De Sanctis, F. Maggio, M. Ruggieri, G. Codispoti, and G. Parca, "Q/V-band satellite communication experiments on channel estimation with Alphasat Aldo Paraboni P/L," in *2015 IEEE Aerospace Conference*, 2015, pp. 1–11.

[20] T. Rossi, M. De Sanctis, M. Ruggieri, C. Riva, L. Luini, G. Codispoti, E. Russo, and G. Parca, "Satellite communication and propagation experiments through the alphasat Q/V band Aldo Paraboni technology demonstration payload," *IEEE Aerospace and Electronic Systems Magazine*, vol. 31, no. 3, pp. 18–27, 2016.

[21] A. Gharanjik, B. Shankar M. R., P.-D. Arapoglou, and B. Ottersten, "Multiple Gateway Transmit Diversity in Q/V Band Feeder Links," *IEEE Transactions on Communications*, vol. 63, no. 3, pp. 916–926, 2015.

[22] M. Vu and A. Paulraj, "MIMO Wireless Linear Precoding," *IEEE Signal Processing Magazine*, vol. 24, no. 5, pp. 86–105, 2007.

[23] G. Gallinaro, G. Caire, M. Debbah, L. Cottatellucci, and R. Mueller, "Perspectives of adopting interference mitigation techniques in the context of broadband multimedia satellite systems," in *Proceedings 23rd AIAA Int. Commun. Sat. Syst. Conf. (ICSSC 2005)*, 2005, pp. 1–8.

[24] P.-D. Arapoglou, K. Liolis, M. Bertinelli, A. Panagopoulos, P. Cottis, and R. De Gaudenzi, "MIMO over Satellite: A Review," *IEEE Communications Surveys Tutorials*, vol. 13, no. 1, pp. 27–51, 2011.

[25] N. Zorba, M. Realp, and A. I. Perez-Neira, "An improved partial CSIT random beamforming for multibeam satellite systems," in *2008 10th International Workshop on Signal Processing for Space Communications*, 2008, pp. 1–8.

[26] P.-D. Arapoglou, A. Ginesi, S. Cioni, S. Erl., F. Clazzer, S. Andrenacci, and A. Vanelli-Coralli, "DVB-S2x enabled precoding for high through-

put satellite systems," *Int. J. Satellite Commun. Netw.*, vol. 34, pp. 439–455, 2015.

[27] D. Christopoulos, P.-D. Arapoglou, and S. Chatzinotas, "Linear precoding in multi-beam SatComs: practical constraints," in *Proc. 31st AIAA Int Commun Sat Syst Conf (ICSSC 2013)*, 2013, pp. 1–8.

[28] G. Zheng, S. Chatzinotas, and B. Ottersten, "Generic Optimization of Linear Precoding in Multibeam Satellite Systems," *IEEE Transactions on Wireless Communications*, vol. 11, no. 6, pp. 2308–2320, 2012.

[29] D. Christopoulos, S. Chatzinotas, G. Taricco, M. Angel Vazquez, A. Perez-Neira, P.-D. Arapoglou, and A. Ginesi, "Chapter 3 - Multibeam joint precoding: frame-based design," in *Cooperative and Cognitive Satellite Systems*, S. Chatzinotas, B. Ottersten, and R. De Gaudenzi, Eds. Academic Press, 2015, pp. 83–118.

[30] M. Poggioni, M. Berioli, and P. Banelli, "BER Performance of Multibeam Satellite Systems with Tomlinson-Harashima Precoding," in *2009 IEEE International Conference on Communications*, 2009, pp. 1–6.

[31] S. Chatzinotas, G. Zheng, and B. Ottersten, "Joint Precoding with Flexible Power Constraints in Multibeam Satellite Systems," in *2011 IEEE Global Telecommunications Conference - GLOBECOM 2011*, 2011, pp. 1–5.

[32] V. Joroughi, M. B. Shankar, S. Maleki, S. Chatzinotas, J. Grotz, and B. Ottersten, "On-Board Precoding in a Multiple Gateway Multibeam Satellite System," in *2018 IEEE 88th Vehicular Technology Conference (VTC-Fall)*, 2018, pp. 1–5.

[33] M. Ángel Vázquez, A. Pérez-Neira, and M. Ángel Lagunas, "Linear precoding in multibeam satellite under licensed shared access," in *2014 7th Advanced Satellite Multimedia Systems Conference and the 13th Signal Processing for Space Communications Workshop (ASMS/SPSC)*, 2014, pp. 312–317.

[34] D. Spano, S. Chatzinotas, J. Krause, and B. Ottersten, "Symbol-level precoding with per-antenna power constraints for the multi-beam satellite downlink," in *2016 8th Advanced Satellite Multimedia Systems Conference and the 14th Signal Processing for Space Communications Workshop (ASMS/SPSC)*, 2016, pp. 1–8.

[35] G. Taricco and A. Ginesi, "Precoding for Flexible High Throughput Satellites: Hot-Spot Scenario," *IEEE Transactions on Broadcasting*, vol. 65, no. 1, pp. 65–72, 2019.

[36] M. A. Vázquez and A. I. Pérez-Neira, "Spectral clustering for beam-free satellite communications," in *2018 IEEE Global Conference on Signal and Information Processing (GlobalSIP)*, 2018, pp. 1030–1034.

[37] V. Joroughi and C. Mosquera, "The impact of feeder link interference in multiple gateway multibeam satellite systems," in *2016 8th Advanced Satellite Multimedia Systems Conference and the 14th Signal Processing for Space Communications Workshop (ASMS/SPSC)*, 2016, pp. 1–8.

[38] G. Taricco, "Linear Precoding Methods for Multi-Beam Broadband Satellite Systems," in *European Wireless 2014; 20th European Wireless Conference*, 2014, pp. 1–6.

[39] B. Devillers, A. Perez-Neira, and C. Mosquera, "Joint Linear Precoding and Beamforming for the Forward Link of Multi-Beam Broadband Satellite Systems," in *2011 IEEE Global Telecommunications Conference - GLOBECOM 2011*, 2011, pp. 1–6.

[40] Y. C. B. Silva and A. Klein, "Linear Transmit Beamforming Techniques for the Multigroup Multicast Scenario," *IEEE Transactions on Vehicular Technology*, vol. 58, no. 8, pp. 4353–4367, 2009.

[41] M. Vázquez, A. Pérez-Neira, D. Christopoulos, S. Chatzinotas, B. Ottersten, P.-D. Arapoglou, A. Ginesi, and G. Taricco, "Precoding in Multibeam Satellite Communications: Present and Future Challenges," *IEEE Wireless Communications*, vol. 23, no. 6, pp. 88–95, 2016.

[42] W. Wang, A. Liu, Q. Zhang, L. You, X. Gao, and G. Zheng, "Robust Multigroup Multicast Transmission for Frame-Based Multi-Beam Satellite Systems," *IEEE Access*, vol. 6, pp. 46 074–46 083, 2018.

[43] A. Guidotti and A. Vanelli-Coralli, "Clustering strategies for multicast precoding in multibeam satellite systems," *International Journal of Satellite Communications and Networking*, vol. 38, no. 2, pp. 85–104, 2020.

[44] A. Guidotti and A. Vanelli-Coralli, "Geographical Scheduling for Multicast Precoding in Multi-Beam Satellite Systems," in *2018 9th Advanced Satellite Multimedia Systems Conference and the 15th Signal Processing for Space Communications Workshop (ASMS/SPSC)*, 2018, pp. 1–8.

[45] A. Guidotti and A. Vanelli-Coralli, "Design Trade-Off Analysis of Precoding Multi-Beam Satellite Communication Systems," in *2021 IEEE Aerospace Conference*, 2021, pp. 1–12.

[46] T. Delamotte, R. T. Schwarz, K.-U. Storek, and A. Knopp, "MIMO Feeder Links for High Throughput Satellites," in *WSA 2018; 22nd International ITG Workshop on Smart Antennas*, 2018, pp. 1–8.

[47] T. Delamotte, K.-U. Storek, and A. Knopp, "MIMO Processing for Satellites in the 5G Era," in *2019 IEEE 2nd 5G World Forum (5GWF)*, 2019, pp. 629–635.

[48] P. Angeletti, R. De Gaudenzi, R. Re, and N. Jeannin, "Multibeam satellite communication system and method, and satellite payload for carrying out such a method," U.S. Patent WO2 014 001 837A1, 2014.

[49] T. de Cola, A. Ginesi, G. Giambene, G. C. Polyzos, V. A. Siris, N. Fotiou, and Y. Thomas, *Network and Protocol Architectures for Future Satellite Systems*, 2017.

[50] "Ieee standard for a precision clock synchronization protocol for networked measurement and control systems," *IEEE Std 1588-2019 (Revision ofIEEE Std 1588-2008)*, pp. 1–499, 2020.

[51] C. Caini, G. Corazza, G. Falciasecca, M. Ruggieri, and F. Vatalaro, "A spectrum- and power-efficient EHF mobile satellite system to be integrated with terrestrial cellular systems," *IEEE Journal on Selected Areas in Communications*, vol. 10, no. 8, pp. 1315–1325, 1992.

[52] R. Muharar and J. Evans, "Downlink Beamforming with Transmit-Side Channel Correlation: A Large System Analysis," in *2011 IEEE International Conference on Communications (ICC)*, 2011, pp. 1–5.

[53] "Propagation data and prediction methods required for the design of Earth-space telecommunication systems," Recommendation ITU-R P.618-13, 2017.

[54] "Attenuation by atmospheric gases and related effects," Recommendation ITU-R P.676-12, 2019.

[55] "Reference standard atmospheres," Recommendation ITU-R P.835-6, 2017.

[56] "Water vapour: surface density and total columnar content," Recommendation ITU-R P.836-6, 2017.

[57] "Attenuation due to clouds and fog," Recommendation ITU-R P.840-8, 2019.

[58] "Characteristics of precipitation for propagation modelling," Recommendation ITU-R P.837-7, 2017.

[59] "Rain height model for prediction methods," Recommendation ITU-R P.839-4, 2013.

[60] "Topography for Earth-space propagation modelling," Recommendation ITU-R P.1511-2, 2019.

[61] "Specific attenuation model for rain for use in prediction methods," Recommendation ITU-R P.838-3, 2005.

[62] *Digital Video Broadcasting (DVB); Implementation guidelines for the second generation system for Broadcasting, Interactive Services, News Gathering and other broadband satellite applications; Part 2: S2 Extensions (DVB-S2X)*, ETSI TR 102 376-2 Std., 2015.

[63] U. Mengali and N. D'Andrea, *Synchronisation Techniques for Digital Receivers*. Springer ed., 1997.

[64] Kay, S. M., *Fundamentals of Statistical Signal Processing: Estimation Theory*. Prentice Hall Signal Processing Series, 1993.

[65] Delamotte, T., *MIMO Feeder Links for Very High Throughput Satellite Systems*. Ph. D. Dissertation, University of Munich, 2019.

Alessandro Guidotti received the master degree (magna cum laude) in telecommunications engineering and the Ph.D. degree in electronics, computer science, and telecommunications from the University of Bologna, Italy, in 2008 and 2012, respectively. From 2014 to 2021, hew was a Research Associate with the Department of Electrical, Electronic, and Information Engineering "Guglielmo Marconi," University of Bologna. From 2021, he is a Researcher with the Consorzio Inter-Universitario delle Telecomunicazioni (CNIT), located at the Research Unit of the University of Bologna. He is active in national and international research projects on wireless and satellite communication systems in several European Space Agency and European Commission funded projects. He is a member of the Editorial Board as Review Editor of the Space Communications journal for Frontiers in Space Technologies. He has been serving as TPC and Publication Co-Chair at the ASMS/SPSC Conference since the 2018 edition. His research interests include wireless communication systems, spectrum management, cognitive radios, interference management, 5G, and Machine Learning.

Claudio Sacchi (Senior Member, IEEE) received the Laurea Degree in Electronic Engineering, and the Ph.D. in Space Science and Engineering at the University of Genoa (Italy) in 1992 and 2003, respectively. From 1996 to 2002, he has been research cooperator with the University of Genoa, Dept. of Biophysical and Electronic Engineering (DIBE) and with the National Italian Consortium in Telecommunications (CNIT), managing project activities in the field of multimedia surveillance systems and satellite communications. Since August 2002, Dr. Sacchi has joined the Department of Information Engineering and Computer Science (DISI) of the University of Trento (Italy), covering the role of assistant professor. He upgraded to the position of associate professor in December 2020. Claudio Sacchi is author and co-author of more than 110 papers published in international journals and conferences. In 2011, he was guest editor of the special issue of PROCEEDINGS OF THE IEEE: Aerospace Communications: History, Trends and Future. Moreover, in 2015, he was guest editor of the featured-topic special issue of IEEE COMMUNICATIONS MAGAZINE: Toward the Space 2.0 Era. Since 2019, Dr. Sacchi has been coordinating and chairing the IEEE AESS technical panel: "Glue Technologies for Space Systems" that was awarded by AESS as "Outstanding Panel of the year 2020". The research interests of Dr. Sacchi are mainly focused on wideband mobile and satellite transmission systems based on space, time and frequency diversity; MIMO systems; array processing; multi-rate and multi-access wireless communications; EHF broadband aerospace communications; software radio and cognitive radio; radio communications for emergency recovery applications. Claudio Sacchi is a senior member of IEEE and a member of the IEEE ComSoc, IEEE BTS, IEEE VT and IEEE AESS society.

Alessandro Vanelli-Coralli (Senior Member, IEEE) received the Dr.Ing. degree in electronics engineering and the Ph.D. degree in electronics and computer science from the University of Bologna, Italy, in 1991 and 1996, respectively. In 1996, he joined the University of Bologna, where he is currently an Associate Professor. He chaired the Ph.D. Board, Electronics, Telecommunications and Information Technologies from 2013 to 2018. From 2003 to 2005, he was a Visiting Scientist with Qualcomm Inc., San Diego, CA, USA. He participates in national and international research projects on wireless and satellite communication systems and he has been a Project Coordinator and scientific responsible for several European Space Agency and European Commission funded projects. He is currently the Responsible for the Vision and Research Strategy task force of the Networld2020 SatCom Working Group. He is a member of the Editorial Board of the Wiley InterScience Journal on Satellite Communications and Networks and Associate Editor of the Editorial Board of Aerial and Space Networks Frontiers in Space Technologies. Dr. Vanelli-Coralli has served in the organisation committees of scientific conferences and since 2010 he is the general CoChairman of the IEEE ASMS Conference. He is co- recipient of several the Best Paper Awards and he is the recipient of the 2019 IEEE Satellite Communications Technical Recognition Award.